I. THE MAGNETIC RESONANCE OF TRIPLET EXCITONS IN SOLID FREE RADICALS

II. A ZERO FIELD MAGNETIC RESONANCE SPECTROMETER

Thesis by

Donal D. Thomas

In Partial Fulfillment of the Requirements

For the Degree of

Doctor of Philosophy

California Institute of Technology

Pasadena, California

1964

ACKNOWLEDGEMENTS

I gratefully acknowledge the advice and help of my scientific advisor, Professor H. M. McConnell. During my years of graduate study he proposed many interesting problems which greatly contributed to my scientific knowledge.

Dr. A. F. Hildebrandt's advice on the electronic phases of my research as well as many helpful conversations on scientific and non-scientific subjects is greatly appreciated.

I am grateful to Professor C. A. Mead and Dr. D. W. Halford for discussions on electronic problems.

I am indebted to the Institute and the National Science Foundation for financial aid during my graduate studies.

ABSTRACT

Part I

The magnetic resonance of triplet excitons in solid free radicals has been studied in both zero magnetic field and a high magnetic field. A discussion of the spin Hamiltonian for triplet excitons in zero field and high field is presented. Calculations of the second moment of the exciton resonances is given and compared for the two cases. The fine-structure splittings of triplet excitons in Wurster's blue perchlorate in a high magnetic field and in $(\phi_3 AsCH_3)^+(TCNQ)_2^-$ in zero field have been determined and their temperature dependence is discussed. The temperature dependence of the line width is also given.

Part II

A zero field magnetic resonance spectrometer has been constructed for use in the 10 - 100 Mc/sec frequency range. A marginal oscillator and bidirectional square wave field modulation are used.

TABLE OF CONTENTS

PART I

THE MAGNETIC RESONANCE OF TRIPLET EXCITONS IN SOLID FREE RADICALS

A. INTRODUCTION

McConnell and Lynden-Bell suggested that at absolute zero many pure solid free radicals are diamagnetic (1, 2). This diamagnetism results from the orderly pairing up of adjacent free radicals to form dimers which have an electronic singlet state and a low lying triplet state. Above absolute zero the triplet state becomes thermally populated, and these triplet excitations can then propagate through the crystal as an exciton wave (2).

The high field magnetic resonance spectra of triplet excitons are characterized by several features. There is a complete absence of hyperfine structure, this being averaged out by the exciton motion (3). At low temperatures where the exciton concentration is small, the spectra consist of two sharp lines with a separation dependent on the zero field splittings of the exciton triplet state. At higher temperatures the lines broaden due to exciton-exciton exchange interaction, and at still higher temperatures where the exciton concentration is large these lines coalesce into one sharp line at $g = 2$.

The magnetic resonance spectra of triplet excitons in a solid free radical were first observed by Chesnut and Phillips (4) and Chesnut and Arthur (5) in the TCNQ free radical salts. Triplet excitons were later observed by McConnell, Pooley and Bradbury in Wurster's blue perchlorate and a preliminary experimental study has been reported (6).

Section I-B discusses the triplet state spin Hamiltonian in the case where there is zero magnetic field and in the case where there is a high magnetic field.

Section I-C describes a calculation of the second moment of the triplet exciton resonance lines in both zero magnetic field and a high magnetic field. These calculations are to a large extent due to Professor McConnell and are included here for the sake of completeness.

Section I-D describes detailed work on the high field magnetic resonance of excitons in Wurster's blue perchlorate. This project was the joint effort of Professor Harden McConnell, Dr. Heimo Keller, and the author.

Section I-E consists of an article to be published on the zero field magnetic resonance of triplet excitons in the $(\phi_3 AsCH_3)^+ (TCNQ)_2^-$ solid free radical salt. The experimental work was carried out by A. W. Merkl and the author. The higher frequency transitions (160 and 220 Mc/sec) and the low frequency transition (60 Mc/sec) were observed by the former and latter respectively. The spectrometer used in the 60 Mc/sec study is described in Part II.

B. TRIPLET STATE SPIN HAMILTONIAN

Zero Magnetic Field

In zero magnetic field the triplet state electron spin-spin (dipole-dipole) interaction is given by

$$\mathcal{H}_{dd} = \sum_{i<j} g^2\beta^2 \frac{\vec{S}_i \cdot \vec{S}_j |r_{ij}|^2 - 3(\vec{S}_i \cdot \vec{r}_{ij})(\vec{S}_j \cdot \vec{r}_{ij})}{|r_{ij}|^5} \qquad \text{(B-1)}$$

where

$\vec{S}_i$ = spin angular momentum operator for electron i,

$\vec{r}_{ij}$ = position vector connecting electron i and j

g = free-electron g-factor

β = Bohr magneton

It has been shown that equation (B-1) can be replaced (in an appropriate coordinate axis system determined by the molecule) by the spin Hamiltonian (7, 8),

$$\mathcal{H}_{dd} = DS_z^2 + E(S_x^2 - S_y^2). \qquad \text{(B-2)}$$

By substituting

$$S_x = \frac{S_+ + S_-}{2} \qquad \text{and} \qquad S_y = \frac{S_+ - S_-}{2i}$$

where S_+ and S_- are the electron raising and lowering operators respectively, equation (B-2) can be written in the form

$$\mathcal{H} = DS_z^2 + \frac{E}{2}(S_+^2 + S_-^2) \qquad \text{(B-3)}$$

Using the following basis states

$$|1\rangle = \alpha\,\alpha \qquad \text{(B-4a)}$$

$$|0\rangle = \frac{\alpha\beta + \beta\alpha}{2} \tag{B-4b}$$

$$|-1\rangle = \beta\beta \tag{B-4c}$$

where α and β are the electron spin up and spin down functions respectively and where the first spin function refers to one electron and the second spin function refers to the other electron, the following energy matrix is obtained,

$$\begin{array}{c} \\ |1\rangle \\ |0\rangle \\ |-1\rangle \end{array} \begin{array}{c} \begin{array}{ccc} |1\rangle & |0\rangle & |-1\rangle \end{array} \\ \begin{pmatrix} D-\varepsilon & 0 & E \\ 0 & -\varepsilon & 0 \\ E & 0 & D-\varepsilon \end{pmatrix} \end{array} \tag{B-5}$$

From this matrix the following eigenenergies and eigenfunctions are found:

$$\varepsilon_1 = D + E \qquad \phi_1 = \frac{|1\rangle + |-1\rangle}{\sqrt{2}} = \frac{\alpha\alpha + \beta\beta}{\sqrt{2}} \tag{B-6a}$$

$$\varepsilon_2 = D - E \qquad \phi_2 = \frac{|1\rangle - |-1\rangle}{\sqrt{2}} = \frac{\alpha\alpha - \beta\beta}{\sqrt{2}} \tag{B-6b}$$

$$\varepsilon_3 = 0 \qquad \phi_3 = |0\rangle = \frac{\alpha\beta + \beta\alpha}{\sqrt{2}} \tag{B-6c}$$

The transition probabilities between these levels are proportional to the square of the matrix elements of the form

$$\langle \phi_i | \mu_k | \phi_j \rangle \tag{B-7}$$

where $i, j = 1, 2, 3$; $k = x, y, z$; and

$$\mu = g_o \beta S \tag{B-8}$$

The non-zero transition probabilities are calculated to be

$$\begin{aligned} |\langle \phi_2 | \mu_z | \phi_1 \rangle|^2 &= g_o^2 \beta^2 \\ |\langle \phi_3 | \mu_x | \phi_1 \rangle|^2 &= g_o^2 \beta^2 \\ |\langle \phi_3 | \mu_y | \phi_2 \rangle|^2 &= g_o^2 \beta^2 \end{aligned} \qquad \text{(B-9)}$$

For an allowed transition the subscript on μ refers to the direction of the polarization of the RF field needed to produce a transition, e.g. in order to produce a transition between states ϕ_2 and ϕ_1 a RF magnctic field of frequency 2E polarized in the z direction is needed. Thus in zero magnetic field the triplet electron resonance spectra will consist of three lines at 2E, D − E, and D + E and polarized in the z, y, and x directions respectively.

High Magnetic Field (3,000 gauss)

In a high magnetic field the spin Hamiltonian for the triplet state can be given by the zero field Hamiltonian (equation B-2) and a high field Zeeman term. Thus in a high magnetic field

$$\begin{aligned} \mathcal{H} &= \mathcal{H}_{\text{Zeeman}} + \mathcal{H}_{\text{dd}} \\ &= |\beta| \vec{H} \cdot g \cdot \vec{S} + DS_z^2 + E(S_x^2 - S_y^2) \end{aligned} \qquad \text{(B-10)}$$

where $\vec{H}$ is the magnetic field and g is the g factor tensor. If g is assumed to be isotropic, equation (B-10) becomes

$$\mathcal{H} = g \beta \left[H_z S_z + H_x S_x + H_y S_y \right] + DS_z^2 + E(S_x^2 - S_y^2) \qquad \text{(B-11)}$$

Using the wave functions given in equation (B-6) as a basis, and letting $H_x = H_y = 0$, $H_z = H$, the following energy matrix is obtained

$$\begin{array}{c} \\ \phi_1 \\ \phi_2 \\ \phi_3 \end{array} \begin{array}{c} \begin{array}{ccc} \phi_1 & \phi_2 & \phi_3 \end{array} \\ \begin{pmatrix} D+E-\varepsilon & g\beta H & 0 \\ g\beta H & D-E-\varepsilon & 0 \\ 0 & 0 & 0-\varepsilon \end{pmatrix} \end{array} \qquad \text{(B-12)}$$

The eigenvalues of the above matrix are found to be

$$\varepsilon_o = 0$$

$$\varepsilon_{\pm} = D \pm \sqrt{(g\beta H)^2 + E^2} \qquad \text{(B-13a)}$$

In a similar way the magnetic energies of the triplet state with the magnetic field in the x and y directions can be found. These energies are

for $H_x = H, \quad H_z = H_y = 0$

$$\varepsilon_o = D - E \qquad \text{(B-13b)}$$

$$\varepsilon_{\pm} = 1/2(D + E) \pm \sqrt{(g\beta H)^2 + 1/4(D + E)^2}$$

for $H_y = H, \quad H_x = H_z = 0$

$$\varepsilon_o = D - E \qquad \text{(B-13c)}$$

$$\varepsilon_{\pm} = 1/2(D - E) \pm \sqrt{(g\beta H)^2 + 1/4(D - E)^2}$$

In a high magnetic field where the strongly allowed transitions are given by $\Delta m = 1$, the resonance spectra will consist of two lines centered about $g\beta H = h\nu$ where ν is the frequency of the spectrometer being used in the experiment. The separation of the two lines will depend upon the relative orientation of the magnetic field with the molecular axes, and for the three principal directions x, y, and z the splittings are respectively, $|D - 3E|$, $|D + 3E|$, and $|2D|$.

The above method of calculating triplet splittings in high field is exact. However it is quite difficult to calculate the splitting with the field direction in an arbitrary orientation using this method. Alternately if $|D|$ and $|E|$ are assumed to be small compared to $g\beta H$ (a condition which is met in the triplet exciton systems to be discussed later), the following method can be used in calculating the separation of the high field electron spin resonance lines of the triplet state.

Let the direction of the high magnetic field be described by the polar coordinates θ, ϕ in the coordinate system defined by equation (B-11). Let a new Cartesian coordinate system (primed system) be defined in the following way. z' is in the direction of the magnetic field and x' remains at all times in the xy plane. Under these conditions the following equations hold:

$$S_z = S_{z'}\cos\theta - S_{y'}\sin\theta \qquad \text{(B-14a)}$$

$$S_x = S_{z'}\sin\theta\cos\phi + S_{x'}\sin\phi + S_{y'}\cos\theta\cos\phi \qquad \text{(B-14b)}$$

$$S_y = S_{x'}\sin\theta\cos\phi - S_{x'}\cos\phi + S_{y'}\cos\theta\sin\phi \qquad \text{(B-14c)}$$

Using equation (B-14) and assuming an isotropic g-factor, equation (B-11) may be rewritten in terms of the primed coordinate system.

$$\begin{aligned} S_z^2 &= S_{z'}^2\cos^2\theta + S_{y'}^2\sin^2\theta \\ &\quad + \text{terms involving } S_{z'}S_{y'} \text{ and } S_{y'}S_{z'} \\ &= S_{z'}^2\cos^2\theta + \frac{\sin^2\theta}{2}(S_{x'}^2 + S_{y'}^2) \\ &\quad - \frac{\sin^2\theta}{2}(S_{x'}^2 - S_{y'}^2) + \ldots \end{aligned} \qquad \text{(B-15)}$$

$$= \frac{1}{2} S_{z'}{}^2 (3\cos^2\theta - 1) + \text{terms}$$

$$\text{involving } (S_{x'}{}^2 - S_{y'}{}^2),\ S_{z'}S_{y'},\ S_{y'}S_{z'}, \text{ and } S^2.$$

$$S_x{}^2 - S_y{}^2 = S_{z'}{}^2 \sin^2\theta(\cos^2\phi - \sin^2\phi) \qquad \text{(B-16)}$$

$$+ S_{x'}{}^2 (\sin^2\phi - \cos^2\phi)$$

$$+ S_{y'}{}^2 \cos^2\theta(\cos^2\phi - \sin^2\phi)$$

$$+ \text{terms involving } S_{x'}S_{z'},\ S_{z'}S_{x'},\ S_{z'}S_{y'},$$

$$S_{y'}S_{z'}, \text{ and } (S_{x'}S_{y'} - S_{y'}S_{x'})$$

$$= S_{z'}{}^2 \sin^2\theta(\cos^2\phi - \sin^2\phi)$$

$$+ \frac{1}{2} (S_{x'}{}^2 + S_{y'}{}^2)(1 - \cos^2\theta)(\sin^2\phi - \cos^2\phi)$$

$$+ \frac{1}{2} (S_{x'}{}^2 - S_{y'}{}^2)(1 + \cos^2\theta)(\sin^2\phi - \cos^2\phi)$$

$$+ \ . \ . \ .$$

$$= \frac{3}{2} S_{z'}{}^2 \sin^2\theta(\cos 2\phi)$$

$$+ \text{terms involving } (S_x{}^2 - S_y{}^2),\ S^2,\ . \ . \ .$$

Therefore in the primed coordinate system,

$$\mathcal{H} = g\beta H S_{z'} + \left[\frac{1}{2}(3\cos^2\theta - 1)D + \frac{3}{2}(\sin^2\theta\cos 2\phi)E\right] S_{z'}{}^2 + \text{terms} \qquad \text{(B-17)}$$

$$\text{involving } (S_{x'}{}^2 - S_{y'}{}^2),\ S^2,\ S_{x'}S_{z'},$$

$$S_{z'}S_{x'},\ S_{y'}S_{z'},\ S_{z'}S_{y'}, \text{ and } (S_{x'}S_{y'} + S_{y'}S_{x'}).$$

In the case where $|D|,\ |E| << g\beta H$, first order perturbation methods can be used to calculate the dipolar contribution to the energy of a triplet state in a high magnetic field. These corrections will be given by the matrix elements of the form

$$\langle i | \mathcal{H}_{dd} | i \rangle \qquad \text{(B-18)}$$

where i = $|1\rangle$, $|0\rangle$, or $|-1\rangle$ as defined in equation (B-4). The only terms in equation (B-17) contributing to these matrix elements is the $S_{z'}^2$ term. The energy of states $|1\rangle$ and $|-1\rangle$ is raised by an amount $\left[\frac{1}{2}(3\cos^2\theta - 1)D + \frac{3}{2}(\sin^2\theta\cos 2\phi)E\right]$ and the energy of state $|0\rangle$ is unchanged. Therefore, the splitting (d) of the two electron spin resonance lines in a high field triplet spectrum is given by

$$d = \left|(3\cos^2\theta - 1)D + 3(\sin^2\theta\cos 2\phi)E\right| \qquad \text{(B-19)}$$

C. TRIPLET EXCITON LINE SHAPE CALCULATIONS

High Magnetic Field

Van Vleck gives the following formula for the calculation of the second moment of a magnetic resonance (9).

$$\langle \nu^2 \rangle = \frac{-\mathrm{Tr}[\mathcal{H}, S_x]^2}{\mathrm{Tr}\,[S_x^2]} \tag{C-1}$$

where $\langle \nu^2 \rangle = \int_0^\infty \nu^2 g(\nu) d\nu$

$\mathcal{H}$ = Hamiltonian for the system and includes only those terms which give rise to first order transitions, i.e., neglects all terms which allow harmonic transitions.

$g(\nu)$ = line shape function of the resonance line

The Hamiltonian for a triplet exciton in a high magnetic field can be approximated by

$$\mathcal{H} = \nu \sum_{i=1}^{N} S_{iz} + D' \sum_{i=1}^{N} S_{iz}^2 + J \sum_{i=1}^{N} S_i \cdot S_{i+1} \tag{C-2}$$

where

$$D' = \frac{1}{2}(3\cos^2\theta - 1)D + \frac{3}{2}(\sin^2\theta \cos 2\phi)E$$

J = exchange interaction between excitons

Noting that $S_x = \sum_{i=1}^{N} S_{ix}$,

$$[\mathcal{H}, S_x] = \frac{\nu}{2} \sum_{i=1}^{N} [S_{i+} - S_{i-}] + \frac{D'}{2} \sum_{i=1}^{N} [2(S_{i+} - S_{i-})S_{iz} + S_{i+} + S_{i-}] \tag{C-3}$$

Squaring and taking the trace

$$\langle \nu^2 \rangle = \nu^2 + D'^2 \tag{C-4}$$

The fourth moment of a magnetic resonance spectra may be calculated using the following equation (9),

$$\langle \nu^4 \rangle = \frac{\mathrm{Tr}\,[\mathcal{H}, U]^2}{\mathrm{Tr}\,[S_x^2]} \tag{C-5}$$

where

$$U = [\mathcal{H}, S_x]$$

from equations (C-2) and (C-3)

$$\begin{aligned}
[\mathcal{H}, U] = {} & \frac{\nu^2}{2}\sum_{i=1}^{N}[S_{i+} + S_{i-}] \\
& + \nu D' \sum_{i=1}^{N}[2(S_{i+} + S_{i-})S_{iz} + S_+ - S_-] \\
& + \frac{D^2}{2}\sum_{i=1}^{N}[4(S_{i+} + S_{i-})S_{iz}^2 + 4(S_{i+} - S_{i-})S_z \\
& \qquad + (S_{i+} + S_{i-})] \\
& + \frac{\nu J}{2}\sum_{i=1}^{N}\{S_{i+1,z}(S_{i+} + S_{i-}) + S_{iz}(S_{i+1,+} + S_{i+1,-})] \\
& + \frac{D'J}{2}\sum_{i=1}^{N}\{S_{i+1,z}[2(S_{i+} + S_{i-})S_{iz} + S_{i+} - S_{i-}] \\
& \qquad + S_{iz}[2(S_{i+1,+} + S_{i+1,-})S_{i+1,z} + S_{i+1,+} - S_{i+1,-}]\} \\
& + \frac{\nu J}{4}\sum_{i=1}^{N}\{[S_{i+1,+} + S_{i+1,-}][S_{i-}S_{i+} - S_{i+}S_{i-}] \\
& \qquad + [S_{i+} + S_{i-}][S_{i+1,-}S_{i+1,+} - S_{i+1,+}S_{i+1,-}]\} \\
& + \frac{D'J}{4}\sum_{i=1}^{N}\{[S_{i+1,+} + S_{i+1,-}][2(S_{i-}S_{i+} - S_{i+}S_{i-})S_{iz} \\
& \qquad + S_{i-}S_{i-} + S_{i-}S_{i+}]
\end{aligned} \tag{C-6}$$

$$+ \left[S_{i+} + S_{i-}\right] \left[2(S_{i+1,-}S_{i+1,+} - S_{i+1,+}S_{i+1,-})S_{i+1,z} + S_{i+1,+}S_{i+1,-} + S_{i+1,-}S_{i+1,+}\right]\Big\}$$

$$-\frac{D'J}{4}\sum_{i=1}^{N}\left[S_{i+1,+}S_{i-}{}^{2} + S_{i+1,-}S_{i+}{}^{2} + S_{i+}S_{i+1,-}{}^{2} + S_{i-}S_{i+1,+}{}^{2}\right]$$

Squaring and taking the trace one finds

$$\langle \nu'^4 \rangle = \nu'^4 + 6\nu'^2 D'^2 + D'^4 + \frac{16}{3} D'^2 J^2 \qquad \text{(C-7)}$$

Alternately one may calculate the left sides of equations (C-1) and (C-5) in the following manner.

The high field magnetic resonance spectra of triplet excitons at low temperatures consist of two lines symmetrically located about the point $\nu'_o = g\beta H$ and separated by $2D'$.

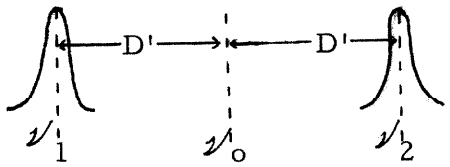

The line shape function $g(\nu')$ may be expressed in the following way,

$$g(\nu') = g_1(\nu') + g_2(\nu') \qquad \text{(C-8)}$$

where $g_1(\nu')$ and $g_2(\nu')$ are the line shape functions of lines 1 and 2 respectively and

$$\int g_1(\nu')d\nu' = \int g_2(\nu')d\nu' = 1 \qquad \text{(C-9)}$$

$$\langle \nu'^2 \rangle = \frac{1}{2}\int \nu'^2 g(\nu')d\nu' \qquad \text{(C-10)}$$

$$= \frac{1}{2}\int (\nu' - \nu_o)^2 g(\nu')d\nu'$$

$$+ \nu_o \int \nu' g(\nu')d\nu' - \nu_o^2$$

The factor of 1/2 comes from the definition in equation (C-9).

$$\langle \Delta\nu'^2 \rangle \equiv \int (\nu' - \nu_o)^2 g(\nu')d\nu' \qquad \text{(C-11)}$$

$$= \int (\nu' - \nu_o)^2 [g_1(\nu') + g_2(\nu')]\, d\nu'$$

$$= \int [(\nu' - \nu_1') + (\nu_1' - \nu_o)]^2 g_1(\nu')d\nu'$$

$$+ \int [(\nu' - \nu_2') + (\nu_2' - \nu_o)]^2 g_2(\nu')d\nu'$$

$$= \int (\nu' - \nu_1')^2 g_1(\nu')d\nu' + 2(\nu_1' - \nu_o)\int (\nu' - \nu_1')g_1(\nu')d\nu'$$

$$+ (\nu_1' - \nu_o)^2 + \int (\nu' - \nu_2')^2 g_2(\nu')d\nu'$$

$$+ 2(\nu_2' - \nu_o)\int (\nu' - \nu_2')g_2(\nu')d\nu' + (\nu_2' - \nu_o)^2$$

Since the lines are symmetric about ν_o

$$\langle \Delta\nu'^2 \rangle = 2\langle \Delta\nu_1'^2 \rangle - 4D'\delta\nu_1' + 2D'^2 \qquad \text{(C-12)}$$

where

$$\langle \Delta\nu_1'^2 \rangle = \int (\nu' - \nu_1')^2 g_1(\nu')d\nu'$$

$$\delta\nu_1' = \int (\nu' - \nu_1')g_1(\nu')d\nu'$$

$$\int \nu g(\nu)d\nu = \int (\nu - \nu_1)g_1(\nu)d\nu + \int \nu_1 g_1(\nu)d\nu \qquad \text{(C-13)}$$

$$+ \int (\nu - \nu_2)g_2(\nu)d\nu + \int \nu_2 g_2(\nu)d\nu$$

$$= \nu_1 + \nu_2 = 2\nu_o$$

since $\int (\nu - \nu_1)g_1(\nu)d\nu = -\int (\nu - \nu_2)g_2(\nu)d\nu$

Combining equations (C-10), (C-12) and (C-13)

$$\langle \nu^2 \rangle = \langle \Delta\nu_1^2 \rangle - 2D'\delta\nu_1 + D'^2 + \nu_o^2 \qquad \text{(C-14)}$$

Equating equation (C-4) and (C-14)

$$\langle \Delta\nu_1^2 \rangle - 2D'\delta\nu_1 = 0$$

$$\delta\nu_1 = \frac{\langle \Delta\nu_1^2 \rangle}{2D'} \qquad \text{(C-15)}$$

In a similar manner one obtains for the 4th moment

$$\langle \Delta\nu^4 \rangle = \langle \Delta\nu_1^4 \rangle \qquad \text{(C-16)}$$

$$+ 2(\nu_1 - \nu_2)\langle \Delta\nu_1^3 \rangle$$

$$+ 3(\nu_1^2 - \nu_2^2)\langle \Delta\nu_1^2 \rangle$$

$$+ 2(\nu_1^3 - \nu_2^3)\delta\nu_1$$

$$+ \frac{1}{2}(\nu_1^4 - \nu_2^4)$$

where $\langle \Delta\nu_1^n \rangle = \int (\nu - \nu_1)^n g_1(\nu)d\nu$

Substituting $\nu_1 = \nu_o - D' \qquad \nu_2 = \nu_o + D'$

$$\langle \Delta\nu^4 \rangle = \langle \Delta\nu_1^4 \rangle - 4D'\langle \Delta\nu_1^3 \rangle + 6(\nu_o^2 - D'^2)\langle \Delta\nu_1^2 \rangle - 4(3\nu_o^2 D' - D'^3)\delta\nu_1 + \nu_o^4 + 6\nu_o^2 D'^2 + D'^4 \qquad \text{(C-17)}$$

Equating equation (C-7) and equation (C-17) noting equation (C-15),

$$\langle \Delta\nu_1^4 \rangle - 4D'\langle \Delta\nu_1^3 \rangle - (4D'^2)\langle \Delta\nu_1^2 \rangle = (16/3)D'^2 J^2 \qquad \text{(C-18)}$$

Since the first two terms on the left side of equation (C-18) are small compared to the third term

$$\langle \Delta\nu_1^2 \rangle = (4/3)J^2 \qquad \text{(C-19)}$$

Zero Magnetic Field

In zero field one may calculate the second moment of a given transition using an equation similar to equation (C-1). In zero field the triplet exciton Hamiltonian is given by

$$\mathcal{H} = D\sum_{i=1}^{N} S_{iz}^2 + E\sum_{i=1}^{N}(S_{ix}^2 - S_{iy}^2) + J\sum_{i}^{N} S_i \cdot S_{i-1} \qquad \text{(C-20)}$$

In the case where J = 0, the energy levels and eigenfunctions are

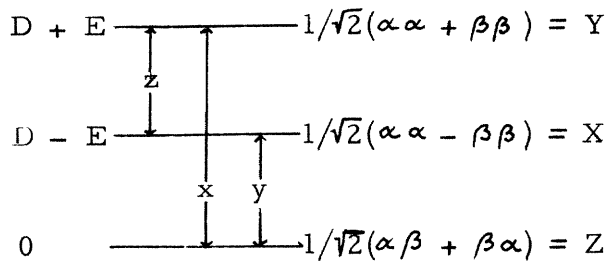

Where the x, y, and z refer to the polarization of the transitions and X, Y, and Z refer to the manner in which the state transforms.

The exchange term on the right side of equation (C-20) includes terms which do not conserve energy. For an example $S_{iz}S_{i+1,z}$ will take the state where the i-th excitation and i + 1st excitation are both in X and put them in Y, i.e.,

$$S_{iz}S_{i+1,z}|X(i)X(i+1)\rangle = |Y(i)Y(i+1)\rangle \qquad \text{(C-22)}$$

If these terms in the Hamiltonian are included in equation (C-1), contributions to the second moment from harmonic transitions will be included in the calculation. To separate out these terms one may define the following set of operators.

$$R_{ij},\ R_{ij}^{\dagger} \text{ where } i = 1 \text{ to } N,\quad j = x, y, z \qquad \text{(C-23)}$$

R_{iz} removes an excitation from state X on site i and puts an excitation in state Y on site i. $R_{iz}^{\dagger}$ removes an excitation from state Y on site i and puts an excitation in state X on site i. The other operators are defined in a similar way using a cyclic permutation of x, y, and z. In zero field

$$\begin{aligned} S_x &= R_x^{\dagger} + R_x \\ S_y &= R_y^{\dagger} + R_y \\ S_z &= R_z^{\dagger} + R_z \end{aligned} \qquad \text{(C-24)}$$

Substituting equation (C-24) into equation (C-20) and neglecting all exchange terms not conserving energy, e.g., $R_{ix}R_{jx}$, etc.,

$$\mathcal{H}' = D\sum_{i=1}^{N}\left[R_{iz}^{\dagger}R_{iz} + R_{iz}R_{iz}^{\dagger}\right] \tag{C-25}$$
$$+ E\sum_{i=1}^{N}\left[R_{ix}^{\dagger}R_{ix} + R_{ix}R_{ix}^{\dagger} - R_{iy}^{\dagger}R_{iy} - R_{iy}R_{iy}^{\dagger}\right]$$
$$+ J\sum_{i=1}^{N}\left[R_{ix}^{\dagger}R_{jx} + R_{ix}R_{jx}^{\dagger} + R_{iy}^{\dagger}R_{jy} + R_{iy}R_{jy}^{\dagger}\right.$$
$$\left. + R_{iz}^{\dagger}R_{jz} + R_{iz}R_{jz}^{\dagger}\right]$$

For the X⟶Y transition one must substitute S_z for S_x in equation (C-1). Therefore the second moment for the z polarized transition becomes

$$\langle \nu^2 \rangle = \frac{-\,\mathrm{Tr}\left[\mathcal{H}', (R_z + R_z^{\dagger})\right]^2}{\mathrm{Tr}\left[R_z + R_z^{\dagger}\right]^2} \tag{C-26}$$

$$\left[\mathcal{H}', (R_z + R_z^{\dagger})\right] = 2E\sum_{i=1}^{N}\left[R_{iz} - R_{iz}^{\dagger}\right] \tag{C-27}$$
$$+ J\sum_{i=1}^{N}\left\{\left[R_{i+1,z} - R_{i+1,z}^{\dagger}\right]\left[R_{iz}^{\dagger}R_{iz} - R_{iz}R_{iz}^{\dagger}\right]\right.$$
$$\left. + \left[R_{iz} - R_{iz}^{\dagger}\right]\left[R_{i+1,z}^{\dagger}R_{i+1,z} - R_{i+1,z}R_{i+1,z}^{\dagger}\right]\right\}$$

Squaring and taking the trace

$$\langle \nu^2 \rangle = 4E^2 + (4/3)J^2 \tag{C-28}$$

Alternately one may calculate

$$\langle \nu^2 \rangle = \int \nu^2 g(\nu)\,d\nu$$

where $$\int g(\nu)d\nu = 1$$

The z polarized transition in zero field consists of one line at frequency $2E \equiv \nu_E$

$$\int \nu^2 g(\nu) d\nu = \int (\nu - \nu_E)^2 g(\nu) d\nu + 2\nu_E \int \nu g(\nu) d\nu - \nu_E^2 \tag{C-29}$$

One may calculate $\int \nu g(\nu) d\nu = \langle \nu \rangle$ (the first moment) using the formula given by Slichter (10)

$$\langle \nu \rangle = \frac{\sum_{E_a > E_b} \langle a | \mu_z | b \rangle \langle b | \mu_z | a \rangle (E_a - E_b)}{\frac{1}{2} \mathrm{Tr}[\mu_z^2]} \tag{C-30}$$

where a, b refer to states in the system and E_a and E_b are their respective energies. Since μ_z can move an excitation from X to Y (or Y to X) on only one site at a time

$$E_a - E_b\Big|_{E_a > E_b} = 2E + E_{a'} - E_{b'} \tag{C-31}$$

where the primed energies refer to the exchange part of the energy.

$$\sum_{E_a > E_b} \langle a | \mu_z | b \rangle \langle b | \mu_z | a \rangle (E_a - E_b) \tag{C-32}$$

$$= \sum_{E_a > E_b} \langle a | \mu_z | b \rangle \langle b | \mu_z | a \rangle 2E + \sum_{E_a > E_b} \langle a | \mu_x | b \rangle \langle b | \mu_z | a \rangle (E_{a'} - E_{b'})$$

The first term on the right hand side of equation (C-32) may be written

$$(2E)\tfrac{1}{2}\mathrm{Tr}[\mu_z^2] \tag{C-33}$$

where the factor of 1/2 is a result of the restriction $E_a > E_b$.

In equation (C-25) the J terms commute with the D and E terms. Therefore, states a and b can be simultaneous eigenfunctions of both the dipolar and exchange parts of the Hamiltonian in equation (C-25). Therefore

$$E_a' = \mathcal{H}_J |a\rangle \tag{C-34a}$$

$$E_b' = \mathcal{H}_J |b\rangle \tag{C-34b}$$

where $\mathcal{H}_J$ is the exchange part of the Hamiltonian in equation (C-25).

Following the method of Slichter, the second term on the right hand side of equation (C-32) becomes

$$\sum_{E_a > E_b} \langle a | [\mathcal{H}_J, \mu_z] | b\rangle\langle b | \mu_z | a\rangle \tag{C-35}$$

The restriction $E_a > E_b$ can be removed by noting $\mu_z = g\beta(R_z + R_z^\dagger)$. Assuming that the energy of state Y is greater than the energy of state X equation (C-35) can be written

$$g^2\beta^2 \sum \langle a | [\mathcal{H}_J, R_z] | b\rangle\langle b | R_z^\dagger | a\rangle \tag{C-36}$$

Since R_z and $R_z^\dagger$ only give contributions to the above expression where $E_a > E_b$. (If state X has a higher energy than state Y, then R_z and $R^\dagger$ are interchanged.) Equation (C-36) then becomes

$$g^2\beta^2 \mathrm{Tr}([\mathcal{H}_J, R_z] R_z^\dagger) \tag{C-37}$$

A calculation of the above trace shows that it vanished. (If R_z and $R_z^\dagger$ are interchanged the result is the same.) Therefore

$$\langle \nu' \rangle = 2E \equiv \nu_E \tag{C-38}$$

Thus equation (C-29) becomes

$$\langle \nu^2 \rangle = \langle \Delta\nu^2 \rangle + \nu_E^2 \qquad \text{(C-39)}$$

Equating equations (C-28) and (C-39)

$$\langle \Delta\nu^2 \rangle = \frac{4}{3} J^2 \qquad \text{(C-40)}$$

Comparing equation (C-19) and equation (C-40) it can be seen that the second moment of one component of the high field magnetic resonance of triplet excitons is identical to the second moment of a zero field transition of triplet excitons.

D. WURSTER'S BLUE PERCHLORATE MAGNETIC RESONANCE IN A HIGH MAGNETIC FIELD

Introduction

The paramagnetic resonance of the positive ion of N, N, N', N' tetramethyl-p-phenylene diamine (the Wurster's blue cation) has been studied extensively. In dilute solution the hyperfine structure pattern extends over a range of more than 300 Mc/sec (11-14), and has now been completely analyzed (15). The solid ionic free radical salt, Wurster's blue perchlorate, shows a sharp exchange narrowed spin resonance line at room temperature, but at lower temperatures there is a broadening of the spin resonance line shape and a marked decrease of spin concentration below 186°K (16-18). This decrease in spin susceptibility also has been seen in static susceptibility measurements (19-22).

McConnell, et al., suggested that the low temperature electronic excitations of Wurster's blue perchlorate might be triplet excitons, which should show characteristic paramagnetic resonance spectra (12, 6). These exciton spectra were apparently not observed in the early resonance work (16-18), presumably because of free radical impurities and also the difficulty of observing the exciton-like spectra in polycrystalline samples (23). The present work gives detailed evidence in support of the earlier suggestion.

The Crystal Structure of Wurster's Blue Perchlorate

Room - Temperature Structure. The room-temperature crystal structure of WB perchlorate has been determined by Turner and Albrecht (TA)(24). They find that room-temperature WB perchlorate is orthorhombic, space group Pn2n or Pnmn, with a unit cell of dimensions $\underset{\sim}{a_o}$ = 5.98Å, $\underset{\sim}{b_o}$ = 10.2Å and $\underset{\sim}{c_o}$ = 10.23Å, which contains two formula units. A projection of the TA structure onto the $\underset{\sim}{a_o}\underset{\sim}{c_o}$ plane is given in figure 1. The WB ions form regular linear chains parallel to the $\underset{\sim}{a_o}$ axis. The long axes of the WB ion molecules lie in the $\underset{\sim}{a_o}\underset{\sim}{c_o}$ plane and make an angle of 37.5° with the $\underset{\sim}{a_o}$ axis, as illustrated in figure 1. There are two linear chains related by a two-fold screw axis. The linear chains are separated by the perchlorate ions; each WB ion is surrounded by six perchlorate ions.

Low-Temperature Structure. It is known that linear chains of equally spaced exchanged-coupled spin S = 1/2 molecules (or atoms) may be unstable with respect to distortions in which the intermolecular distances alternate (25-29). This originally led to the suggestion (1) that a dimerization of the WB ions was responsible for the decrease in magnetic susceptibility of WB perchlorate at 186°K. Some investigators have attributed this decrease in susceptibility to a transition to an antiferromagnetic state (17-19), although Turner and Albrecht (24) suggested that the decrease might be due to a polymerization of the WB ions, and Hausser has found both optical and magnetic evi-

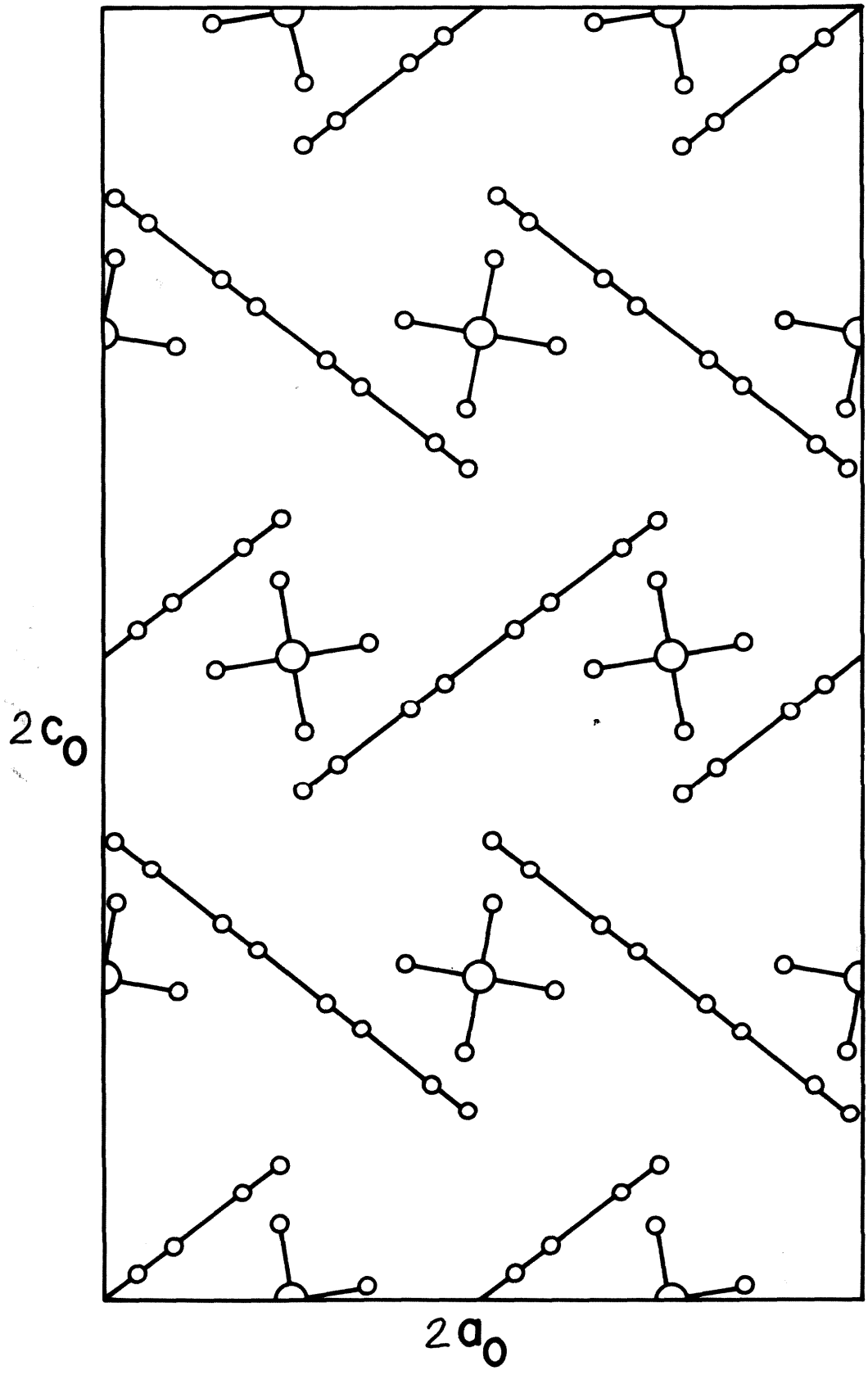

Figure 1. Projection of the orthorhombic structure of Wurster's blue perchlorate onto the $\underset{\sim}{a}_o\underset{\sim}{c}_o$ plane.

dence for a dimerization of WB ions in solution (21, 30, 31) and has suggested the possibility of a dimerization in the solid (11). In order to investigate this proposed low-temperature dimerization a crystal structure study of WB perchlorate at approximately 77°K has been undertaken by Dr. E. Hughes and Professor B. Kamb of this Institute. A preliminary report of their work is given here with their kind permission.

The low-temperature X-ray measurements were carried out by blowing cold nitrogen gas, near the temperature of boiling nitrogen, at a WB single crystal while the diffraction pictures were being taken. At this low temperature the orthorhombic room-temperature cell has changed to a cell of monoclinic symmetry, with a doubling of both the $\underset{\sim}{a}_o$ and $\underset{\sim}{b}_o$ axes. (The orthorhombic→monoclinic transition temperature is probably 186°K, the temperature at which there is a sudden decrease in the magnetic susceptibility (17-22). The cell volume is only doubled since the monoclinic cell has a $\underset{\sim}{C}$-centering translation corresponding to the [110] translation of the orthorhombic parent lattice. The doubling of the cell in the $\underset{\sim}{a}_o$ direction is compatible with the dimerization to give the linear chains of molecular pairs discussed above. The monoclinic form can also be described in terms of a primitive cell having axes $\underset{\sim}{\bar{a}}$, $\underset{\sim}{\bar{b}}$, and $\underset{\sim}{\bar{c}}$. The $\underset{\sim}{n}$-glide plane (001) of the orthorhombic cell becomes a $\underset{\sim}{d}$-glide in the $\underset{\sim}{C}$-centered cell, or an $\underset{\sim}{a}$-glide in the primitive cell. When a single needle-shaped crystal of WB

perchlorate is cooled to 77°K, it becomes a mosaic of twinned domains that share common (0 1 0) planes. That is, there are two differently oriented crystal domains related to one another by a mirror plane (the(0 1 0) plane). The single crystal does not shatter but is easily fractured. The macroscopic needle axis remains the $\underset{\sim}{a}$-axis for the $\underset{\sim}{C}$ cell of both twin components. The cell constants for the monoclinic $\underset{\sim}{C}$-centered cell are $\underset{\sim}{a}'$ = 11.70 ± .01Å, $\underset{\sim}{b}'$ = 20.22 ± .02Å, and $\underset{\sim}{c}'$ = 10.17 ± .04Å, γ = 92.7 ± 0.1°. The relationship between these various unit cells is sketched in figure 2.

In the present discussion the following notation will be used. $\underset{\sim}{a}_o$, $\underset{\sim}{b}_o$, $\underset{\sim}{c}_o$ designate the axes of the orthorhombic (room-temperature) structure, and $\underset{\sim}{a}'$, $\underset{\sim}{b}'$, $\underset{\sim}{c}'$ and $\underset{\sim}{a}''$, $\underset{\sim}{b}''$, $\underset{\sim}{c}''$, designate the monoclinic $\underset{\sim}{C}$-cell axes, where the primes and double primes refer to axes for the two monoclinic twinned domains. The low-temperature twins are assumed to be oriented so that $\underset{\sim}{a}_o = \underset{\sim}{a}' = \underset{\sim}{a}''$ and $\underset{\sim}{c}_o = \underset{\sim}{c}' = \underset{\sim}{c}''$. Note that the labeling of the monoclinic axes differs from the conventional notation in the labeling of the $\underset{\sim}{b}$ and $\underset{\sim}{c}$ axes.

Experimental

All resonance spectra were taken on a Varian Model V4500-10 EPR spectrometer using a Varian Model V4560 100 Kc/sec field modulation unit and a Varian 12 inch electromagnet. The low-temperature spectra were obtained with a metal helium Dewar designed by H. Griffith, D. Wood and A. Kwiram in this laboratory. The micro-

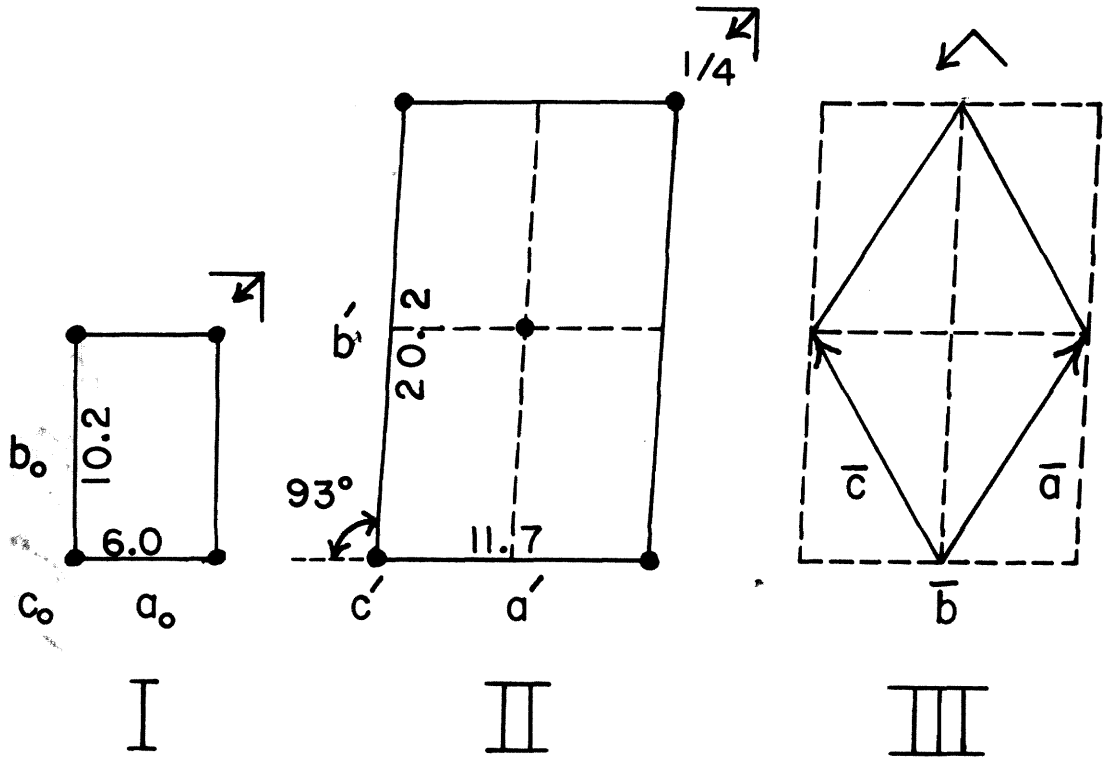

Figure 2. Unit cell structures of Wurster's blue perchlorate. I. Room temperature orthorhombic cell; II. Low temperature (77°K) C-centered monoclinic cell; III. Low temperature monoclinic primitive cell.

wave cavity was attached directly to the inside chamber of the Dewar and kept at the sample temperature. Temperature regulation was achieved by blowing cold helium gas into the inside chamber. The temperature was varied by changing the cold helium gas flow rate. Because of the large heat capacity of the Dewar, the above method of temperature control was very adequate.

The single crystal of Wurster's blue perchlorate used in this experiment was made by H. Keller (32). It was found to be extremely difficult to make single crystals of WB perchlorate large enough to use in a detailed magnetic resonance study. The crystal used in this experiment was obtained after several months of work.

Temperature Dependence of the Magnetic Resonance Spectra

Magnetic resonance spectra were observed in the $\underset{\sim}{a}_o\underset{\sim}{b}_o$, $\underset{\sim}{b}_o\underset{\sim}{c}_o$, and $\underset{\sim}{c}_o\underset{\sim}{a}_o$ planes, i.e., had the WB perchlorate crystal been at room temperature the external strong magnetic field $\underset{\sim}{H}_o$ would have been moving in the $\underset{\sim}{a}_o\underset{\sim}{b}_o$, $\underset{\sim}{b}_o\underset{\sim}{c}_o$ and $\underset{\sim}{c}_o\underset{\sim}{a}_o$ planes. Crystal axes were kindly identified by Dr. E. Hughes using X-ray diffraction. Figure 3 gives spectra for $H_o \| a_o$ in the temperature range 30^o – 74^oK. The central resonance is attributed to a free radical "impurity" in the crystal (see below) and the outer lines are assigned to a fine-structure splitting of the exciton state. The individual fine-structure components have peak-to-peak line widths of the order of 8 Mc/sec at the lower temperatures, much less than that expected from the hyperfine broadening (or split-

Figure 3. Paramagnetic resonance spectra of a Wurster's blue perchlorate crystal at 74°K, 64°K, 45°K and 30°K. The small differences in the line shape of the two fine-structure line in each spectrum are due to slight temperature decreases during the scan of the magnetic field.

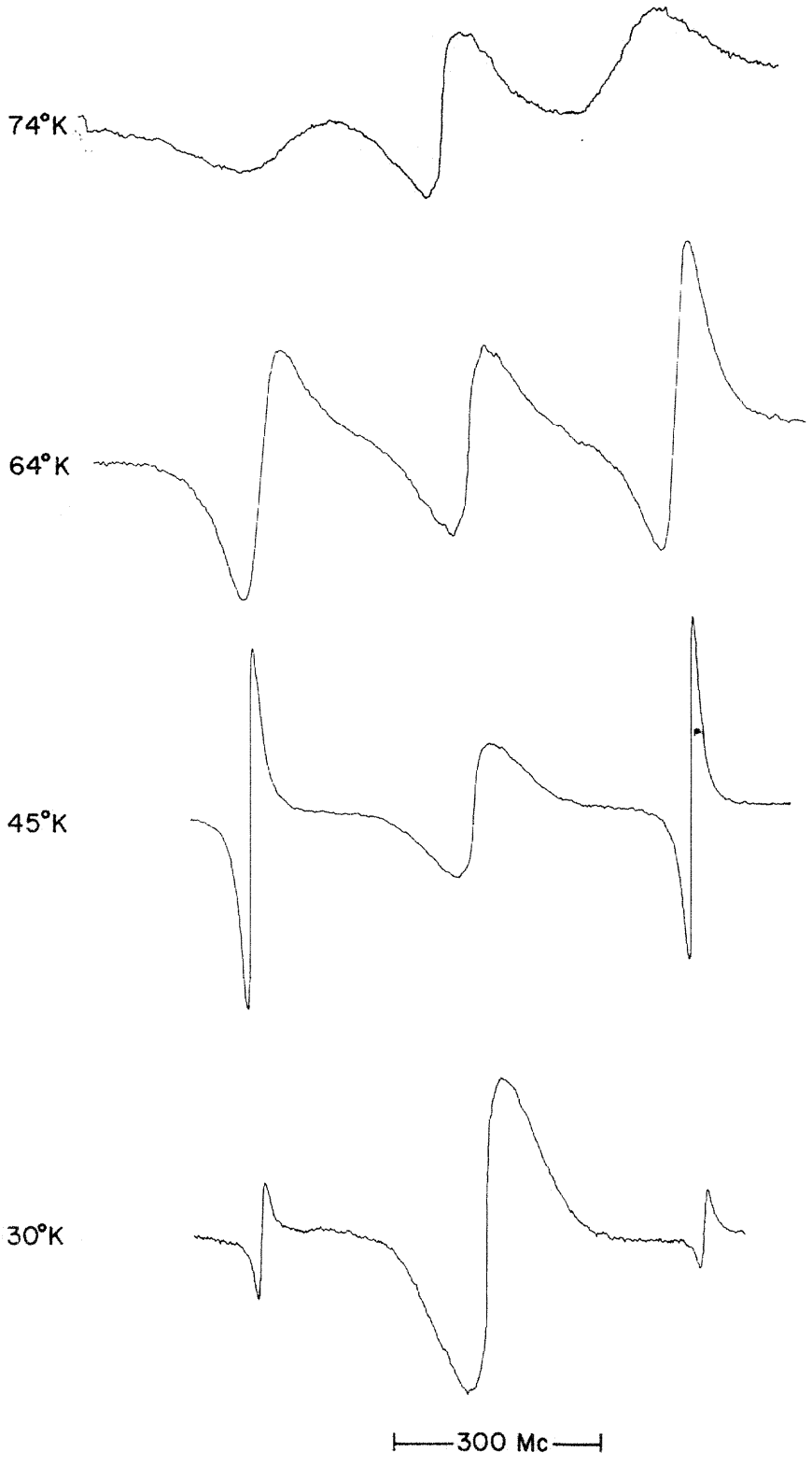
74°K
64°K
45°K
30°K
300 Mc

ting) of the resonance of a single WB ion.

The spectra exhibited in figure 3 shows exciton-exciton exchange broadening with increasing temperature. An "anomalous" broadening similar to that observed by Jones and Chesnut in the TCNQ free radical salts (33) is also found in the WB system. Figure 4(a) shows a plot of log (IT) vs. 1/T where I is the relative integrated fine-structure signal intensity. The singlet-triplet excitation energy J calculated from these data is 246 $\pm$ 20 cm^{-1}. Figure 4(b) shows a plot of logν vs. 1/T where ν is the "exchange frequency" (33) for exciton-exciton spin exchange. For the limit of slow exchange (i.e., where $\nu << \{$separation between the fine structure lines$\}$) this is given by (33)

$$\nu = \sqrt{3}(\Delta\nu - \Delta\nu_0). \qquad \text{(D-1)}$$

$\Delta\nu$ and $\Delta\nu_0$ are the line widths in Mc/sec of one component of the fine-structure spectra measured between the peak points of the derivative of the absorption in the presence and absence of exchange broadening, respectively (33). The activation energy for the exchange is found to be $\Delta E = 392 \pm 20 cm^{-1}$.

Jones and Chesnut (33) have considered that the activation energy for exchange ΔE might exceed the singlet-triplet excitation energy J if the exciton motion were diffusional with activation energy $\epsilon = \Delta E - J$. The "exchange frequency" ν is then expected to be of the order of magnitude,

$$\nu \sim f\tau_c^{-1}, \qquad \text{(D-2)}$$

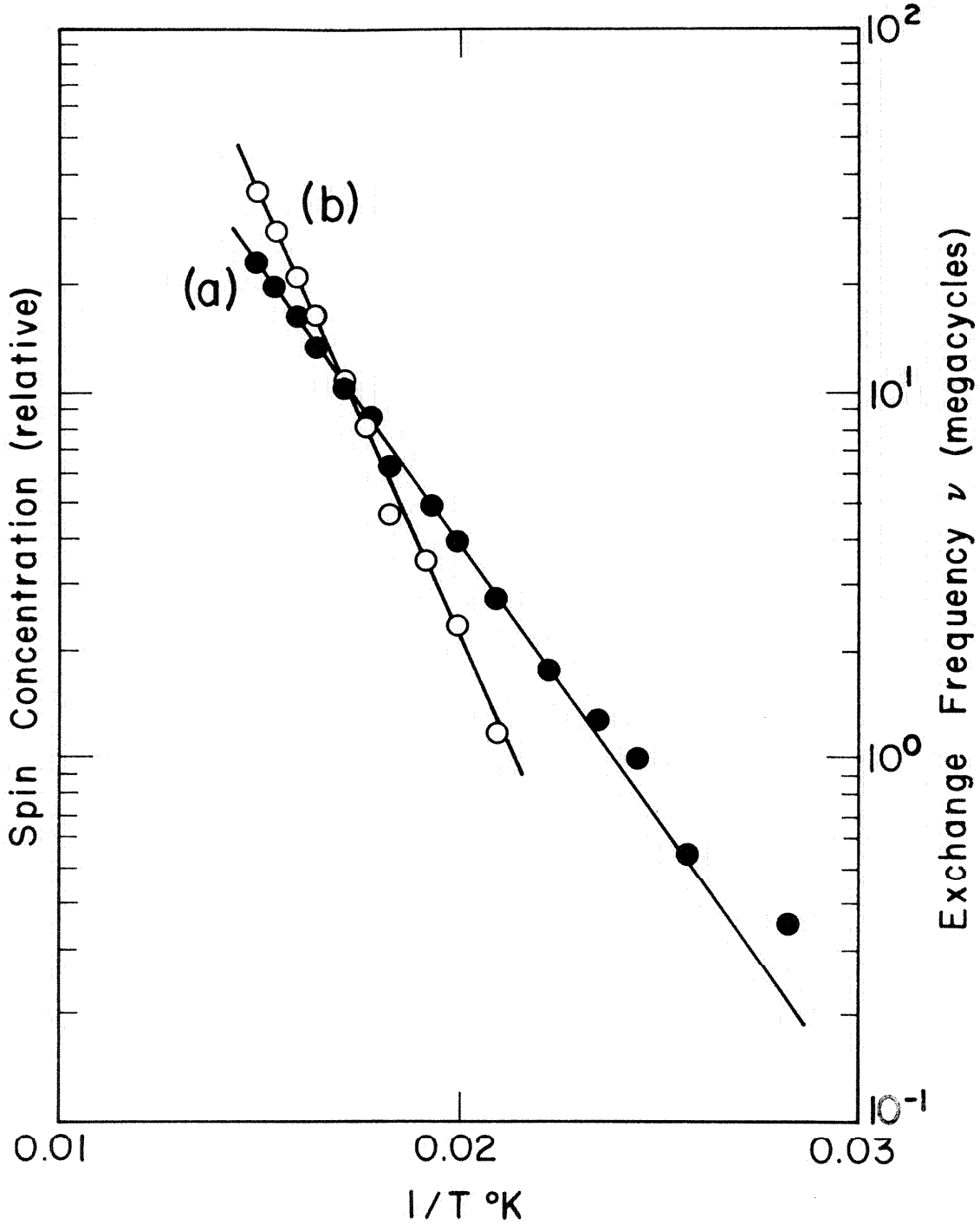

Figure 4 Semilog plot of (a) relative spin concentration and (b) exchange frequency vs. $1/T^{o}K$ for a single crystal of Wurster's blue perchlorate.

where c is the relative triplet-singlet concentration (assumed small), τ is the average time between jumps, and f is the fraction of excitation-excitation collisions that produce a broadening. Equation (D-2) is similar to one given by Pake and Tuttle (34) for spin exchange broadening by radical-radical collisions in solution. If exchange interaction is responsible for exciton motion (2), which is most reasonable but not absolutely certain, then f is certainly of the order of one. In the low-temperature region where $J>>kT$, $C \simeq 3\exp(-J/kT)$. If the supposed diffusional motion has an activation energy ϵ, then

$$\tau^{-1} = \tau_o^{-1}\exp(-\epsilon/kT) \qquad \text{(D-3)}$$

Thus the activation energy for the "exchange frequency" ν is $\Delta E = \epsilon + J$,

$$\nu \simeq 3f\,\tau_o^{-1}\exp(-\Delta E/kT) \qquad \text{(D-4)}$$

This explanation of the origin of the large activation for exchange does not appear consistent with the low-temperature spectra, however. For example, no appreciable broadening of the WB perchlorate spectra at $24^{\circ}K$ was observed. If the excitation were jumping with an activation energy of $\epsilon = 392 - 246 = 146\ cm^{-1}$ from one pair of WB ions to the next, then at $24^{\circ}K$ the jump rate would be only 10 Mc/sec, certainly not enough (1) to remove the known (11-15) nuclear hyperfine splittings. Therefore, there must be some other explanation for the large activation energy for exchange broadening. This problem is discussed below.

The Exciton Spin Hamiltonian

The fine-structure term in the spin Hamiltonian for S = 1 excitons (see equation (B-2)) is sensitive to the rate of exciton jumping between molecular sites which are oriented differently in space (3, 35). Thus, the spin Hamiltonian for excitons in the WB perchlorate crystal is sensitive to the rate of exciton jumping between the pairs of chains related to one another by a glide plane (and two-fold screw axis) in the monoclinic structure. When the applied magnetic field lies in the a'b' plane these chains are magnetically equivalent since the a'b'(= a''b'' = $a_o b_o$) plane is the glide plane of the monoclinic structure. Magnetic equivalence means that for these magnetic field orientations excitons confined to one chain or another would give identical spectra. For this special case the rate of exciton chain jumping has no effect on the fine-structure splittings when the external magnetic field is so strong that the component of spin angular momentum in the field direction S_H is a very good quantum number (3, 35). In the present experiment the applied field is easily large enough to meet the above requirement.

In general, spectra observed in the ab $\equiv$ a'b' $=$ a''b'' $=$ $a_o b_o$ plane are doubled, as illustrated in figure 5. Since the chains in each WB singlet crystal domain are equivalent for these field orientations, but the domains are not, one fine-structure splitting comes from one domain, and the other fine-structure splitting comes from the other domain. A plot of the observed fine-structure splittings is given in figure 6.

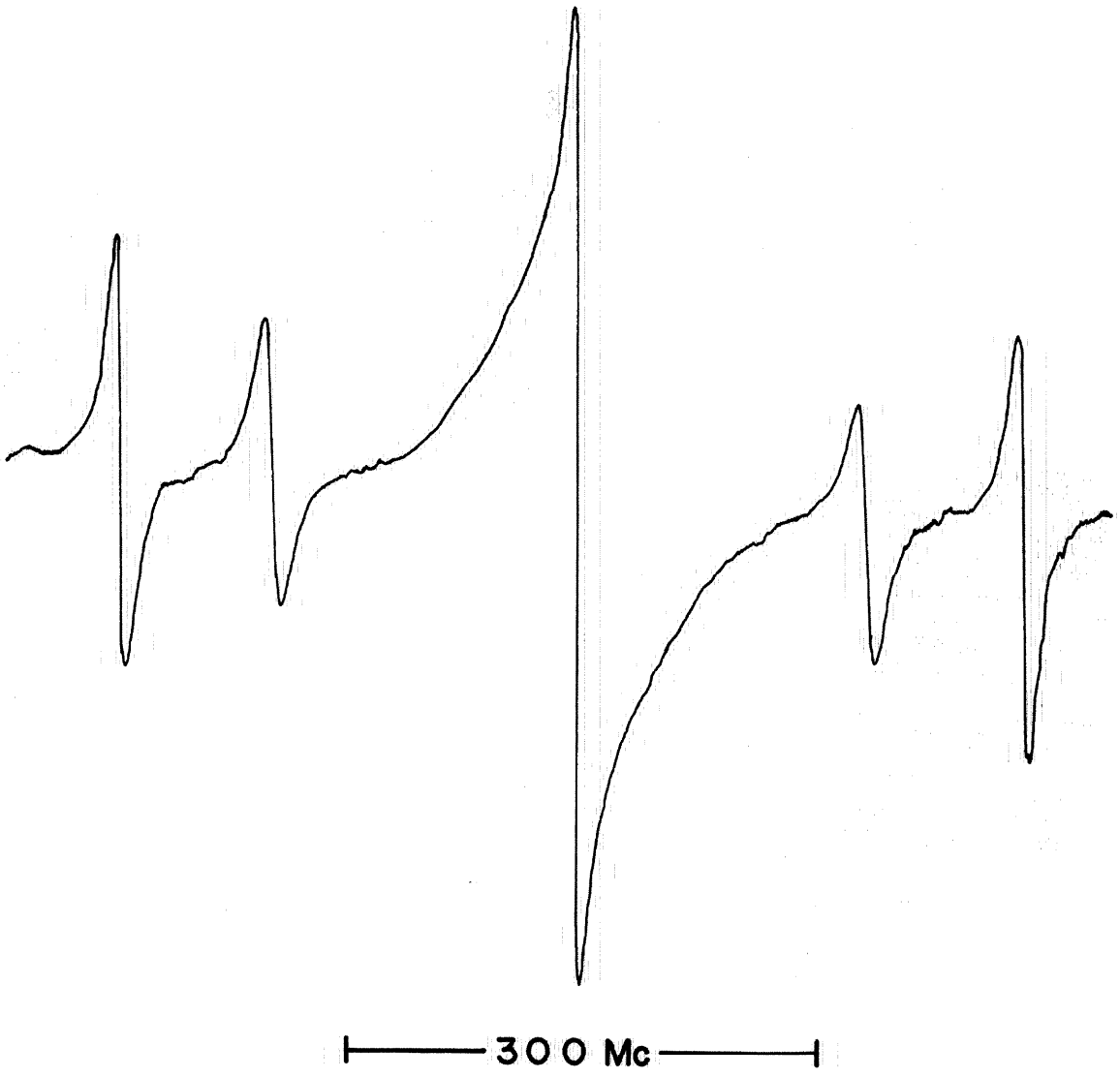

Figure 5 Spectrum of a WB perchlorate crystal H_o is rotated 20^o from $\underset{\sim}{b}_o$ in the $\underset{\sim}{a}_o\underset{\sim}{b}_o$ plane.

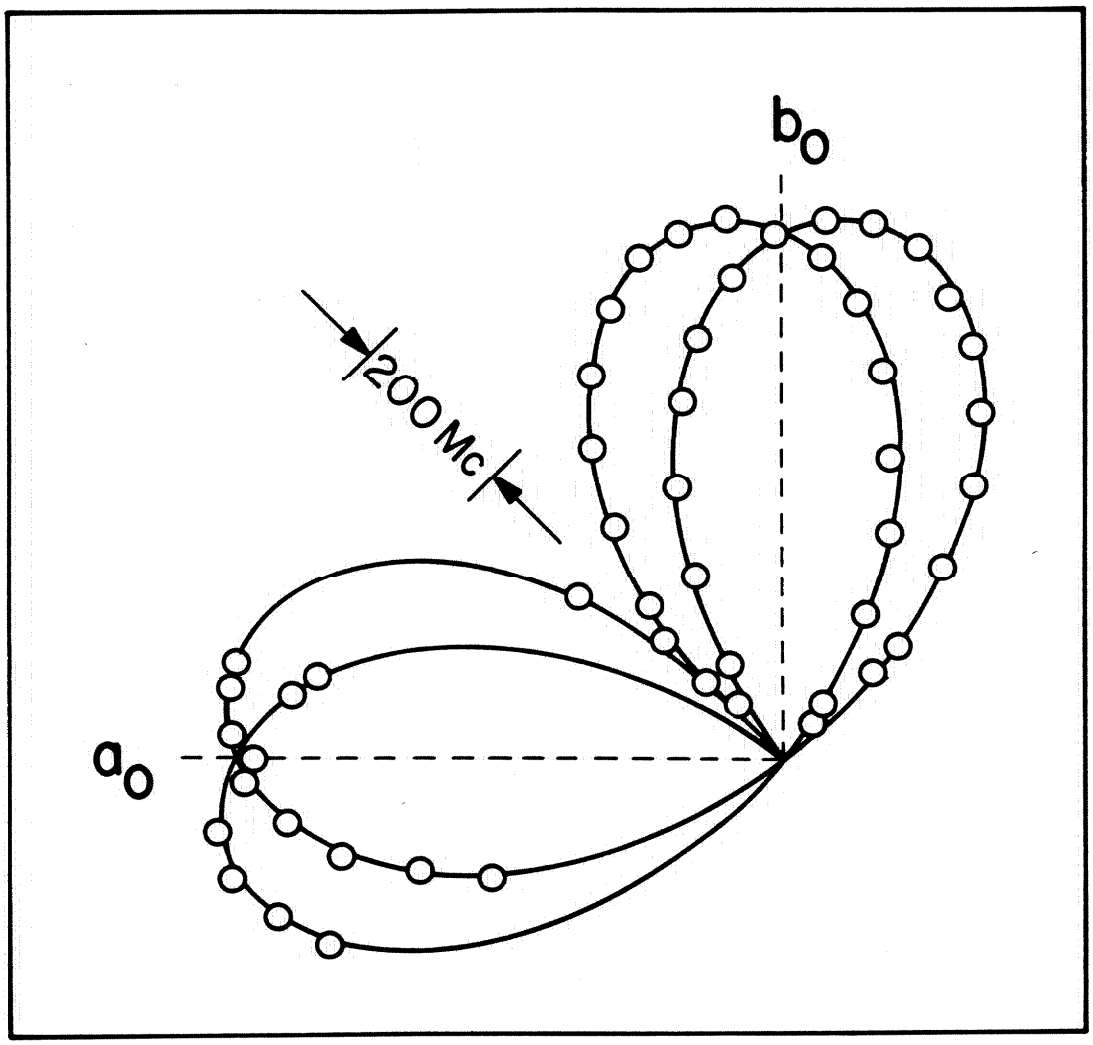

Figure 6. Fine structure splittings in Wurster's blue perchlorate for H_o in the $\tilde{a}_o\tilde{b}_o$ plane. Spectra were taken in the 40 - 45°K temperature range. Solid lines represent polar plots of cos2Ø; circles give experimental splittings.

Although the spectra observed in the $\underset{\sim}{ab}$ plane give no information on the exciton chain-to-chain jump rate, for the sake of discussion assume that the jump rate is very high, so that the excitons are "three-dimensional." Under this assumption the fine-structure Hamiltonian must have the point group symmetry of the crystal structure. Thus in this case the two fold screw axis $\underset{\sim}{c'} = \underset{\sim}{c''} (= \underset{\sim}{c_o})$ must be a principal axis of the fine-structure Hamiltonian, and the other two principal axes lie in the $\underset{\sim}{ab}$ plane. The extrema in figure 6 lie along the principal axes of the two domains. The principal axes of one domain are rotated relative to the principal axes of the other domain by 14 ± 2^{o}. For a single domain the two principal axis splittings in the $\underset{\sim}{ab}$ plane are equal to one another to within 2%. All splittings observed in the $\underset{\sim}{ab}$ plane conform closely to a $|\cos 2\phi|$ angular dependence (see equation (B-19)) as shown in figure 6.

The chains are also equivalent when the external field is parallel to $\underset{\sim}{c_o}$, and here again chain jumping has no effect on the spectra in high field. In this case no detectable splitting was observed.

All of these results can be accounted for by the spin Hamiltonian

$$\mathcal{H} = E(S_x^2 - S_y^2) \qquad \text{(D-5)}$$

where $E = 212 \pm 6$ Mc/sec and where S_x and S_y are the components of spin in the direction of the principal fine-structure axes, designated x and y, where $x = x'$, $y = y'$ for one domain and $x = x''$, $y = y''$ for

the other domain. The third principal axis $z = z' = z''$ is the same for both domains and coincides with the $\underset{\sim}{c}_o$ axis. The axes x' and x'' are chosen closest to a' and a'' respectively.

The Hamiltonian in equation (D-5) is appropriate to three dimensional excitons, even though it was derived from spectra where chain-to-chain jumping does not affect the fine-structure splittings. This Hamiltonian would in general be incorrect for one dimensional excitons since the $\underset{\sim}{c}_o$ axis would not necessarily be a principal axis and the extrema observed for the splittings in the $\underset{\sim}{ab}$ plane need not correspond to principal axes either. On the other hand, if the excitons were one dimensional the Hamiltonian in equation (D-5) could be used to predict a certain average of the fine-structure splittings of the one dimensional excitons.

When the applied field lies in the $\underset{\sim}{b}_o \underset{\sim}{c}_o$ and $\underset{\sim}{a}_o \underset{\sim}{c}_o$ planes, the domains must give identical spectra. The domains are equivalent for a field direction in the $\underset{\sim}{a}_o\underset{\sim}{c}_o$ plane since this is the mirror plane that relates one twin to another. The domains are also equivalent for field directions in the $\underset{\sim}{b}_o\underset{\sim}{c}_o$ plane since these directions are perpendicular to a two-fold axis that rotates one domain into the other. This two-fold axis is parallel to the intersection of the glide plane $\underset{\sim}{ab}$ of the monoclinic structure and the mirror plane $\underset{\sim}{a}_o\underset{\sim}{c}_o$ that reflects one domain into the other.

In the $\underset{\sim}{b}_o\underset{\sim}{c}_o$ plane the two fine-structure lines are broad

(approximately 15 Mc/sec peak-to-peak) at most orientations, and the observed splittings are close to the $3/2\ E \sin^2\theta$ splitting expected from equation (D-5), where θ is the angle between the field direction and the $\underset{\sim}{c}_o$ axis. One expects a $3/2\ E \sin^2\theta$ splitting from a single domain when the field lies in the yz plane of that domain. The y'z' and y''z'' planes only differ from the $\underset{\sim}{b}_o\underset{\sim}{c}_o$ plane by 7^o. Since the two chains in the monoclinic crystal are not equivalent (by symmetry) in the $\underset{\sim}{b}_o\underset{\sim}{c}_o$ plane, the absence of a doubling of the fine-structure lines, as well as conformity of the splittings to equation (D-5), may be due to the fact that (A) the chains are so very nearly equivalent as to not give resolvable splittings, or (B) the excitons jump between the chains at a rate that is large compared to the difference in the fine-structure splittings at these orientations. Later it will be shown that interpretation (B) is to be preferred.

Illustrative spectra observed in the $\underset{\sim}{a}_o\underset{\sim}{c}_o$ plane are given in figure 7. As an inspection of figure 1 suggests, the molecular orientations in the two (room-temperature) chains are magnetically quite different for some field directions in the $\underset{\sim}{a}_o\underset{\sim}{c}_o$ plane, so that large differences in the one-dimensional fine-structure splittings might be expected. Accordingly the interchain jump rate for excitons is apparently not large enough to average out the differences in the fine-structure splittings, so that the fine-structure lines broaden and disappear at crystal orientations in the $\underset{\sim}{a}_o\underset{\sim}{c}_o$ plane where this one-dimensional splitting difference is large. When considering splitting differences,

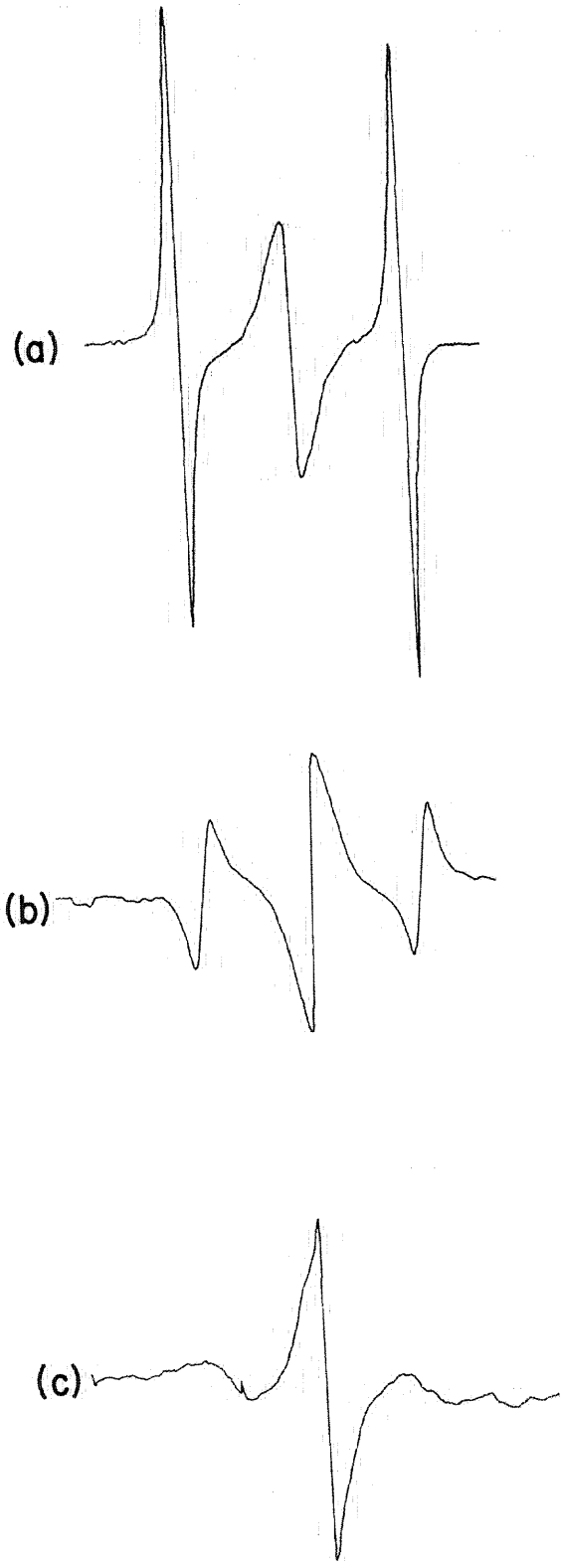

Figure 7. Fine-structure splittings in the $a_o c_o$ plane of Wurster's blue perchlorate. The angle between the field direction and the a_o axis is (a) 0^o, (b) 10^o, (c) 20^o.

the difference in the field value for the resonance of a given spin flip, e.g., $S_H = -1 \rightarrow 0$, for each chain must be considered. Thus it is possible in a four line spectrum to have two sets of slightly split doublets in which the fine-structure splitting difference is very large.

A lower limit on the jump rate can be estimated from the maximum observable line width, i.e., approximately 50 Mc/sec. On the otherhand, the jump rate cannot be much greater than the maximum difference of the fine-structure splittings, which should be no greater than the known fine-structure splittings of triplet states in aromatic molecules, e.g., 3000Mc/sec (36, 37). Also, the theoretical calculations to determine E described later lead to a similar upper limit. These conclusions then show that the spectra observed in the $\underset{\sim}{b}_o\underset{\sim}{c}_o$ plane are indeed true three dimensional exciton spectra, since the chain-to-chain jump rate is 50 Mc/sec or more and the line widths observed in the $\underset{\sim}{b}_o\underset{\sim}{c}_o$ plane are only 15 Mc/sec. Therefore explanation (A) cannot be relevant.

The magnitude of D and E in equation (B-2) can be estimated for WB by the following simple calculation. Equation (B-1) can be written in the form

$$\mathcal{H}_{dd} = \frac{g^2\beta^2}{|r_{12}|^3}\Big\{(1 - 3\cos^2\theta)S_{1z}S_{2z} + (1 - 3\sin^2\theta\cos^2\phi)S_{1x}S_{2x} + (1 - 3\sin^2\theta\sin^2\phi)S_{1y}S_{2y}\Big\} + \text{terms involving} \qquad \text{(D-6)}$$

$$S_{1z}S_{2x},\ S_{1y}S_{2x},\ S_{1z}S_{2y},\ \text{etc.}$$

Making the substitution

$$S_{1i}S_{2i} = \frac{1}{2}(S_i^2 - S_{1i}^2 - S_{2i}^2) \tag{D-7}$$

where i = x, y or z and S_i is the total spin angular momentum operator in the i direction and noting $S_{1x}^2 = S_{2x}^2 = S_{1y}^2 = S_{2y}^2 = S_{1z}^2 = S_{2z}^2 = 1/4$

$$\begin{aligned}\mathcal{H}_{dd} = \frac{g^2\beta^2}{|r_{12}|^3}\Big\{&\frac{1}{2}\left[1 - 3\cos^2\theta\right]S_z^2 \\ &+ \frac{1}{4}\left[2 - 3\sin^2\theta\right]\left[S_x^2 + S_y^2\right] \\ &+ \frac{1}{4}\left[-3\sin^2\theta(\cos^2\phi - \sin^2\phi)\right]\left[S_x^2 - S_y^2\right]\Big\} + \ldots \\ = \frac{g^2\beta^2}{|r_{12}|^3}\Big\{&\frac{3}{4}(1 - 3\cos^2\theta)S_z^2 + \frac{1}{4}\left[2 - 3\sin^2\theta\right]S^2 \\ &+ \frac{1}{4}\left[-3\sin^2\theta(\cos^2\phi - \sin^2\phi)\left[S_x^2 - S_y^2\right]\right\} + \ldots\end{aligned} \tag{D-8}$$

For the same reasons stated in section (I-B) the $S_{iz}S_{jx}$, etc., terms will not contribute to the dipolar energy to first order. Equating equation (D-8) with equation (B-2) the following equations are obtained

$$D = \frac{3}{4}\frac{g^2\beta^2}{|r_{12}|^3}(1 - 3\cos^2\theta) \tag{D-9}$$

$$E = \frac{1}{4}\frac{g^2\beta^2}{|r_{12}|^3}(3\sin^2\theta)(\sin^2\phi - \cos^2\phi) \tag{D-10}$$

In the case of Wurster's blue perchlorate where the spin is distributed over several atoms, the magnitude of D and E can be calculated using the following expressions

$$D = \frac{3}{4}(g^2\beta^2) \sum_{ij} \rho_i \rho_j (1 - 3\cos^2\theta_{ij}) \left| r_{ij} \right|^{-3} \qquad (D\text{-}11)$$

$$E = \frac{1}{4}(g^2\beta^2) \sum_{ij} \rho_i \rho_j (3\sin^2\theta)(\sin^2\phi - \cos^2\phi) \left| r_{ij} \right|^{-3} \qquad (D\text{-}12)$$

where ρ_i and ρ_j are the π-spin densities (38) on atoms i in the first molecule and j in the second molecule, and θ_{ij} is the angle between the $\underset{\sim}{c}_o$ axis and the vector distance $\underset{\sim}{r}_{ij}$ connecting i to j. When one uses the Hückel approximation for ρ_i and ρ_j (with $\alpha_N = \alpha_c$) (39) and takes the θ_{ij} and $\underset{\sim}{r}_{ij}$ to be the same as those found by TA in the orthorhombic crystal, one obtains $D \approx -19$ Mc/sec and $E \approx 186$ Mc/sec. These rough calculations suggest that the WB dimerization which has been assumed to take place in the orthorhombic $\rightarrow$ monoclinic phase change may involve only very small molecular displacements.

Spectroscopic splitting factors were measured by using a free electron cyclotron resonance, for which the g-factor is 2.0000, in the (low pressure) microwave resonance cavity. The measured g-factor parallel to $\underset{\sim}{a}_o$ is 2.0040 ± .0006, and the g-factor parallel to $\underset{\sim}{b}_o$ is 2.0046 ± .0006. An accurate g-factor parallel to $\underset{\sim}{c}_o$ could not be determined because of interference of the "impurity signal" (see below), but the g-factor is certainly of the order of 2.00.

Impurity Signal

In the low temperature WB perchlorate spectra illustrated in figures 3, 5 and 7 the central signal near g = 2 apparently is unrelated to the exciton phenomenon. Its intensity appears to deviate

only slightly from Curie's law in the 25 - 60°K range. A plot for the g = 2 signal similar to that given in figure 4a gives an "activation energy" of only approximately 13 cm^{-1}. Since the microwave cavity used was at the same temperature as the sample, systematic (temperature-dependent) variations of instrument sensitivity might possibly account for this apparent deviation from Curie's law.

In this discussion the central signal will be referred to as the "impurity signal." It might well arise from paramagnetic impurities, or indirectly, from diamagnetic impurities in the crystal lattice. In the latter case, a diamagnetic impurity that replaces a WB ion in the crystal leaves a paramagnetic WB ion that cannot pair up in the low-temperature monoclinic form. This unpaired WB ion might be the origin of the impurity signal. Similarly, "misfits" could contribute to the g = 2 signal (1).

In any case a free radical spin that interacts with virtual triplet excitons of the linear chain may show a somewhat narrowed resonance line shape (loss of nuclear hyperfine structure). (On the other hand spin exchange interactions between fixed free radicals and real triplet excitons can give rise to a broadening of the free radical signal (40)). Also, impurity free radicals may interact indirectly with one another through virtual triplet excitons, giving small singlet-triplet splittings of the free radical pairs and small fine-structure splittings.

Discussion

The notion that the elementary electronic excitations of many solid free radicals are triplet excitons (1) is supported by the present work. Previously, the only solid free radicals exhibiting clear evidence of triplet excitons were the TCNQ free radical salts studied by Chesnut and co-workers (4, 5, 33). These TCNQ free radicals differ from WB perchlorate in a number of qualitative respects - the TCNQ free radicals are negative rather than positive ions, and stoichiometrically there is in general less than one free spin per TCNQ molecule (in TCNQ salts giving exciton spectra) rather than one free spin per aromatic ring as in WB perchlorate. The chain-to-chain exciton jumping found here for WB perchlorate - but apparently not yet observed in the TCNQ salts - must clearly be a sensitive function of the crystal structure and the non-radical compensating ions (perchlorate). The path for this chain-to-chain jumping may become evident when the crystal structure of monoclinic WB perchlorate is determined.

The phase transition in WB perchlorate - presumably leading to a dimerization of the WB ions - may have its counterpart in other solid free radicals. Thus Chesnut and Phillips (4) have noted that in unpublished work Kepler has found a discontinuity in the magnetic susceptibility of $(\phi_3 PCH_3)^+(TCNQ)_2^-$ at approximately $315^\circ K$; this salt shows exciton magnetic resonance at lower temperatures (4, 33). Similarly Edelstein and Mandel (17) have found a sharp decrease in

the paramagnetic resonance susceptibility of picrylaminocarbazyl at approximately $80^{o}K$. This solid radical will also probably show triplet exciton magnetic resonance spectra at lower temperatures.

McConnell and Soos (41) have shown that exciton-phonon coupling in solid free radicals leads to a spin independent repulsion between paramagnetic excitons. This repulsion may be responsible for the activation energy for spin-exchange broadening discussed above. They have estimated the repulsion potential to be of the order of 500 cm^{-1}. This value certainly compares very favorably with the value of ϵ in equation (D-3) (146 cm^{-1}).

E. $(\phi_3 AsCH_3)^-(TCNQ)_2^-$ MAGNETIC RESONANCE IN ZERO MAGNETIC FIELD

This section consists of an article to be published on the above subject. The references for this article only are given on pages 63 and 64. The figures for this article are given on pages 65 through 74.

ZERO-FIELD EXCITON MAGNETIC RESONANCE*

D. D. Thomas,† A. W. Merkl,†† A. F. Hildebrandt,†††

and H. M. McConnell†††

Departments of Physics and Chemistry§

California Institute of Technology

Pasadena, California 91109

*The major portion of this work was supported by the United States Atomic Energy Commission, contract AT(04-3) - 475. Preliminary exploratory work was supported by National Science Foundation Grant G19641.

†NSF Predoctoral Fellow

††Supported by AEC contract AT(04-3) - 475

†††Supported for this work primarily by AEC contract AT(04-3) - 475

§Contribution No. 3054

Abstract

The zero-field magnetic resonance spectrum of triplet excitons in the solid ionic free radical $(\phi_3AsCH_3)^+(TCNQ)_2^-$ has been observed in the 75-140°K temperature range using marginal oscillator spectrometers. Zero-field transition frequencies of 61.4 Mc/sec, 163.8 Mc/sec and 225.4 Mc/sec were observed at a temperature of 111°K. The transition frequencies decrease by roughly 0.1-1% per 10° in the 75-130°K range. The transition frequencies are in good agreement with the frequencies that can be calculated from the earlier high-field spectra of this compound obtained by Chesnut and Phillips. At low temperatures where exciton-exciton spin exchange is weak, the dominant temperature dependence of the zero-field transition frequencies is shown to be due to molecular torsional oscillations that are quite similar to those that are known to produce temperature dependent transition frequencies in nuclear quadrupole resonance. In a sample contaminated with spin 1/2 free radicals, small temperature independent frequency shifts are found and are attributed to second-order exciton-free radical spin exchange. An analysis of exciton line widths in terms of an exciton diffusional motion leads to a site-to-site jump rate of the order of $\tau \sim 10^{12}$ sec^{-1}.

Introduction

One common obstacle to the observation of triplet exciton magnetic resonance in solid free radicals is the difficulty of obtaining suitably large single crystals (1) for high-field spectroscopy. This has prompted us to carry out a zero-field magnetic resonance study of triplet excitons. We report here the observation of zero-field exciton magnetic resonance in a polycrystalline solid ionic free radical, $(\phi_3 AsCH_3)^+(TCNQ)_2^-$, which has been studied previously in high fields by Chesnut and Phillips (2) and Jones and Chesnut (3). As is evident from the present study, the zero-field technique is also particularly convenient for the determination of the elements of the exciton fine structure spin Hamiltonian and their temperature dependence. It may be noted that zero-field magnetic resonance has also been used previously to study free radicals produced in organic crystals by x-ray damage (4)(5). This application of the method is severely limited to radicals having a modest number of nuclear hyperfine interactions (5). The nuclear hyperfine structure of triplet excitons is almost completely averaged out by "motional" narrowing (6).

Spin Hamiltonian

In zero-field the spin Hamiltonian $\mathcal{H}_k$ for a linear triplet exciton of wave vector k has the form (7)

$$\mathcal{H}_k = D_k S_{z'}^2 + E_k (S_{x'}^2 - S_{y'}^2) \qquad (1)$$

where D_k and E_k depend on cos k and where k is the exciton "momentum." For experiments where the exciton motion energy (7), J' cos k, is small compared to kT, and where there is rapid scattering among

the k states (short mean free path), the spin Hamiltonian takes the familiar form (7),

$$\mathcal{H} = DS_{z'}^2 + E(S_{x'}^2 - S_{y'}^2) \qquad (2)$$

There are no nuclear hyperfine structure terms since the excitation is presumed to move, or be distributed over such a large number of nuclei that the hyperfine structure is averaged out (6). For subsequent discussions it will be convenient to rewrite the above Hamiltonian in the form

$$\mathcal{H} = XS_x^2 + YS_y^2 + ZS_z^2 \qquad (3)$$

The three eigenstates of $\mathcal{H}$ have energies X + Y, X + Z and Y + Z. The axes x, y, z are chosen so that $X > Y > Z$. The transition frequencies are Y - Z, X - Y and X - Z and are linearly polarized in the directions x, z, and y as shown in Fig. 1. The eigenstates of $\mathcal{H}$ are designated $|x\rangle$, $|y\rangle$ and $|z\rangle$ as indicated in Fig. 1.

Chesnut and Phillips (2) observed high-field splittings in $(\phi_3 AsCH_3)^+(TCNQ)_2^-$ that correspond to transition frequencies of 215.4 Mc/sec, 156.6 Mc/sec and 58.8 Mc/sec. For notational convenience we shall assume these to be the y, x, and z transitions, respectively. (For the axis system x, y, z defined above one can be certain that the highest frequency transition is y-polarized, but the polarizations of the two lower frequency transitions are not fixed by the relative magnitudes of the transition frequencies.)

Experimental

Because of the comparatively large differences in the transition

frequencies, two different marginal oscillators were used. For the 60 Mc/sec transition (z) an oscillator similar to that described by Shulman (8) was used. The higher frequency transitions at 160 Mc/sec (x) and 220 Mc/sec (y) were observed using a marginal oscillator described by LaForce (9). A bidirectional square wave modulation system similar to that of Cole, et al. (5) was employed. The cooling of the sample was accomplished with a gas flow system, nitrogen and helium being used as refrigerants. The frequencies were measured either directly with a Hewlett Packard Model 524C counter or by using the counter in conjunction with a Hewlett Packard Model 540B transfer oscillator.

The accuracy of the experimental work was limited by the following conditions.

a) Temperature Control - Styrofoam provided the thermal insulation around the sample in both spectrometers. The oscillator coil leads in the low frequency spectrometer provided a heat leak resulting in a 2° to 5° temperature gradient across the sample. The heat leaks near the sample in the high frequency spectrometer were somewhat less, the temperature gradient across the sample ranging from 1/2° to 2°. In each case the larger temperature gradients occurred at the higher temperatures when the gas flow was considerably less.

b) Modulation Amplitude - Since the exciton resonance lines broaden with increasing temperature, the upper temperature at which reliable frequencies and line widths could be measured was limited by the available modulation amplitude. As the lines broaden an increasingly larger magnetic field is required to completely erase the resonance. The geometry of the system used at 60 Mc/sec made it

difficult to erase all but the narrowest lines. Since these lines occurred in the lower range of temperature, where the signal to noise was rapidly decreasing, the data taken at the higher frequencies are more reliable.

Observed resonance spectra are given in Figs. 2 and 3. Figure 2 shows the three resonance curves, x, y, z, at 111°K. Note that all absorption curves are Lorentzian and have the same width to within experimental error. Figure 3 shows the effect of increasing temperature on the line width and resonance frequency of the y-transition. Note that with increasing temperature there is a resonance shift to lower frequencies as well as line broadening. Similar shifts and broadenings are observed for the other two transitions.

The temperature dependence of the x- and y-transition frequencies is given in Fig. 4. To within experimental error the z-transition frequency was found to be equal to the difference of the y- and x-transition frequencies. The origin of these temperature dependent frequency shifts will be discussed below.

The observed resonance line widths are given in Fig. 5. The data in Fig. 5 refer to two separate samples, I and II. I was a very pure $(\phi_3 AsCH_3)^+(TCNQ)_2^-$ polycrystalline sample, kindly given to us by Dr. Don Chesnut of the E. I. duPont Co., which contained ca. 0.01% free radical impurity. Sample II was prepared in these laboratories and contained ca. 1% free radical impurity. The TCNQ was kindly prepared for us by Dr. Heimo Keller. The exciton concentration, C, used in preparing Fig. 5, is taken from the equation,

$$C = 3 \exp(-J/kT) \qquad (4)$$

where J is the singlet-triplet "activation energy" reported by Jones and Chesnut (4), J = 0.065 ev. The free radical impurity concentration is measured on the same scale as the exciton concentration. That is, the free radical concentration is equal to that exciton concentration for which the integrated impurity free radical signal is equal to the integrated exciton signal. It will be noted that curve (a) for the pure sample (I) is quite linear, whereas curve (b) for sample II is definitely not.

Frequency Shifts

In this section we discuss the origin of the temperature dependence of the zero-field transition frequencies shown in Fig. 4. First consider exchange contributions to the zero-field transition frequencies.

Exchange Interactions - Exchange interactions between excitons can give rise to shifts of the zero-field transition frequencies with increasing exciton concentration (i.e., increasing temperature). To understand this "exchange shift" qualitatively, let us consider two excitons of spin S = 1 that are coupled by an average "effective" exchange interaction J_{eff} that is small compared to the transition frequencies of the noninteracting excitons, ν_x, ν_y, ν_z. In zero field the spin Hamiltonian for the problem is

$$\mathcal{H} = \sum_{i=1}^{2} XS_{ix}^2 + YS_{iy}^2 + ZS_{iz}^2 + J_{eff} S_1 \cdot S_2 \qquad (5)$$

Here $\nu_x = Y - Z$, $\nu_y = X - Z$, $\nu_z = X - Y$.

The first-order effect of the exchange coupling of the excitons is to split each zero-field resonance into a triplet of equally spaced lines as illustrated in Fig. 7 for the highest frequency transition ν_y. The second-order effects (as seen in Fig. 7) produce a shift to higher frequencies. The average frequency for each of the transitions is readily found by second-order perturbation theory:

$$\bar{\nu}_y = \nu_y + (2\nu_z/\nu_y + \nu_z/\nu_x + 1)J_{eff}^2/6\nu_z \qquad (6)$$

$$= \nu_y + 1.920(J_{eff}^2/6\nu_z)$$

$$\bar{\nu}_x = \nu_x + (2\nu_z/\nu_x + \nu_z/\nu_y - 1)J_{eff}^2/6\nu_z$$

$$= \nu_x + 0.024(J_{eff}^2/6\nu_z)$$

$$\bar{\nu}_z = \nu_z + (\nu_z/\nu_y - \nu_z/\nu_x + 2)J_{eff}^2/6\nu_z$$

$$= \nu_z + 1.896(J_{eff}/6\nu_z)$$

The numerical results above are based on the ratios $(\nu_z/\nu_y) \simeq 60/220$ and $(\nu_z/\nu_x) \simeq 60/160$.

Since increasing temperature corresponds to increasing exciton concentration and increasing the effective exchange interaction J_{eff} between the excitons, the observed decrease of, for example, ν_y with increasing temperature cannot be accounted for by the exchange effect since this effect produces a shift to higher frequencies. Moreover, the order of magnitude of the calculated exchange shift is too small. For example, consider the y-polarized transition in pure sample I in the lower temperature region (80 - 100°K). The experimental value for the temperature dependence of the transition frequency is

$$\left(\frac{1}{\nu}\frac{d\nu}{dT}\right)_{expt} \sim -3 \times 10^{-4}(°K)^{-1} \qquad (7)$$

The exchange contribution to $\frac{1}{\nu}\frac{d\nu}{dT}$

is of the order

$$\left(\frac{1}{\nu}\frac{d\nu}{dT}\right)_{exch.} \sim \frac{2J_{eff}}{\nu^2}\quad\frac{dJ_{eff}}{dT} \tag{8}$$

$$\sim 1.5 \times 10^{-6}(°K)^{-1}$$

in the temperature range 80–100°K where the observed line width is taken equal to J_{eff} (~ 1.5 Mc/sec) and $\frac{dJ_{eff}}{dT}$ is estimated to be $\sim 2 \times 10^{-2}$ Mc/sec/°K from the temperature dependence of the line width. The exchange contribution to the shift must be even less than $1.5 \times 10^{-6}(°K)^{-1}$ since the line width must have contributions other than first-order exchange (see below). Thus in the 80–100°K range, exchange interactions make no significant contribution to the observed temperature dependence of the transition frequencies. In the earlier high-field study of $(\phi_3 AsCH_3)^+(TCNQ)_2^-$ Jones and Chesnut (3) have also noted that the temperature dependence of the fine-structure splitting could not be accounted for in terms of exchange interaction between excitons.

Exchange interactions between spin 1/2 impurity free radicals and triplet excitons can also produce second order exchange shifts. Exchange interactions between excitons and free radical impurities in high-field spectra have been noted previously (10). For example, if we consider a triplet exciton exchange coupled with a free electron spin through a weak exchange interaction J_{eff}, then we may calculate the following average transition frequencies for the exciton–free electron spin complex in zero field:

$$\bar{\nu}_y = \nu_y + 1.920(J_{eff}^2/4\nu_z) \qquad (9)$$

$$\bar{\nu}_x = \nu_x + 0.024(J_{eff}^2/4\nu_z)$$

$$\bar{\nu}_z = \nu_z + 1.896(J_{eff}^2/4\nu_z)$$

The exchange shifts given in the above expressions are based on the frequency ratios $(\nu_z/\nu_x) \simeq 60/160$ and $(\nu_z/\nu_y) \simeq 60/220$. We suggest that the frequency shifts of "dirty" sample II relative to "pure" sample I may be due to second-order exchange interaction between the exciton and impurity free radicals. Unfortunately, this is not simply an exciton-spin 1/2 interaction problem, because for a realistic calculation one must consider the (very complicated) zero-field states of the free radical due to hyperfine interactions. Even the signs of the exchange shifts are difficult to predict when the frequency separations of the zero-field hyperfine states are comparable to those of the triplet exciton, which is very probably the case in the present problem. For zero-field hyperfine states that have separations less than exciton fine-structure states, one does expect a second-order shift of the highest frequency exciton transition to still higher frequencies, as observed.

The data in Fig. 6 suggest that the exchange broadening of the exciton resonance is roughly independent of temperature and exciton concentration. This indicates the absence of a large activation barrier to exciton-free radical exchange interaction. This point is discussed in more detail later.

Exciton Motion - It is shown elsewhere (6) that the spin Hamiltonian, and hence the zero-field transition frequencies, of a triplet exciton depend on the wave vector k. When exciton bands are narrow compared to thermal energies all k-states are populated with nearly equal

probability, and the temperature dependence of the transition frequencies due to this effect can be neglected. We shall assume that the exciton band in $(\phi_3 AsCH_3)^+(TCNQ)_2^-$ is indeed this narrow.

Torsional Molecular Oscillations - The temperature dependence of nuclear quadrupole frequencies in crystals of chlorinated aromatic molecules is qualitatively similar to the temperature dependence of the zero-field transition frequencies of $(\phi_3 AsCH_3)^+(TCNQ)_2^-$ shown in Fig. 4. For example, in the temperature region 170-270°K the chlorine quadrupole resonance frequency in chlorobenzene at 34-34.5 Mc/sec decreases at a rate of the order of $\frac{1}{\nu}\frac{d\nu}{dT} \sim -10^{-4}(°K)^{-1}$(11). This is of the same order as the rate of change in the 80-110°K region of the y-polarized transition frequency in sample I, $\frac{1}{\nu}\frac{d\nu}{dT} \sim -3 \times 10^{-4}$ $(°K)^{-1}$. It is well known (12) that this temperature dependence of the quadrupole frequency in aromatic crystals is due largely to torsional molecular motion, and it is exceedingly likely that this motion is also responsible for most of the temperature dependence of the zero-field transition frequencies seen in Fig. 4 in the 80-110°K region. Since the theory of the effect of torsional motion on nuclear quadrupole frequencies can be carried over to the exciton problem with almost trivial modifications, we shall not present a detailed discussion except to point out that a realistic order-of-magnitude calculation can be made.

For simplicity consider two coaxial benzene negative ions on top of one another, as sketched in Fig. 8, with uniform spin densities of $\rho_i = 1/6$ on each carbon atom. The spin Hamiltonian for this symmetry is of the form DS_z^2, where D is given by the following formula (13) which only includes contributions from nearest neighbor inter-

molecular carbon-carbon pairs.

$$D = \tfrac{3}{4} g^2 \beta^2 \sum_i \rho_i^2 (1 - 3\cos^2\theta_i) R_i^{-3} \qquad (10)$$

Here θ_i is the angle between the instantaneous nearest neighbor intermolecular carbon-carbon vector R_i and the axis of the two rings. Again for simplicity of calculation we take as equilibrium configuration one in which the carbon atoms are directly above one another. Then for small oscillations of the rings about this common axis (θ small) one obtains the following expression,

$$\frac{1}{D}\frac{dD}{dT} = -3\frac{d\langle\theta^2\rangle}{dT} \qquad (11)$$

where $\langle\theta^2\rangle$ denotes the thermal average of θ^2. In the "classical" limit, $kT \gg h\omega$, where ω is the torsional oscillation frequency, $\langle\theta^2\rangle$ is proportional to the absolute temperature (12), $\langle\theta^2\rangle = \lambda T$. The order of magnitude of $\langle\theta^2\rangle$ can be inferred from r.m.s. thermal parameters observed in x-ray diffraction spectra. Although these data are not available for $(\phi_3 AsCH_3)^+(TCNQ)_2^-$, experimental studies on other charge-transfer type crystalline complexes (14) show the mean square deviation of peripheral atoms from their average positions to be as high as 0.08 Å^2 at room temperature. This deviation corresponds to a λ of the order of 0.08/300 or 2.7×10^{-4}. Thus, we obtain the estimate

$$\frac{1}{D}\frac{dD}{dT} \sim -8 \times 10^{-4} (°K)^{-1} \qquad (12)$$

which is in satisfactory order-of-magnitude agreement with the experimental temperature dependence of the zero-field transition frequencies, e.g., $-3 \times 10^{-4} (°K)^{-1}$.

Resonance Line Widths

The temperature dependence of the high-field exciton magnetic resonance line width in $(\phi_3 AsCH_3)^+(TCNQ)_2^-$ has been studied previously by Chesnut and Phillips (2), and Jones and Chesnut (3). In the present section we compare the high-field and zero-field line widths and consider briefly the origin of these widths in terms of exciton structure and motion.

At low temperature (~77°K) the high-field exciton resonance lines are Lorentzian, with line widths in the range 1.1 - 3.3 Mc/sec (15) depending on the crystal orientation relative to the applied field direction. This anisotropy may be due to exciton-nuclear hyperfine interactions that are not completely averaged out by exciton "motion" (16). This hyperfine interaction should not contribute strongly to the zero-field line widths since in zero field the hyperfine interaction is second-order (17), whereas it is first order in high fields. The zero-field width of ~ 1.25 Mc/sec at ~ 77°K is thus consistent with the narrowest high-field width, ~1.1 Mc/sec (15) observed at this temperature, provided the first-order high-field hyperfine interaction can be neglected at this orientation (16).

To understand the possible significance of these results, let us tentatively assume a diffusional model in which a localized exciton hops from site to site on the linear free radical chain with jumping probability τ^{-1}. In a time t the exciton makes t/τ jumps, and moves over a number of distinct sites n, where $n \sim (t/\tau)^{1/2}$. The high-field hyperfine line width W_{hf} of an exciton distributed over n sites is of order $A/n^{1/2}$ where A is the hyperfine line width of an exciton localized on a single site. Thus,

$$W_{hf} \sim A(\tau/t)^{1/4} \tag{13}$$

We set $t = \left(\sqrt{3}\pi W_{hf}\right)^{-1}$ since this is essentially the lifetime of the magnetic state giving the observed resonance. This leads to the result

$$\tau^{-1} = \sqrt{3}\pi A^4/W_{hf}^3 \tag{14}$$

Since A is estimated (6) to be of the order of 30 Mc/sec and W_{hf} above is estimated to be of the order of 1 Mc/sec, we obtain $\tau^{-1} \sim 10^{12}$.

The exciton line broadening at exciton concentrations above $C \sim 10^{-3}$ seen in Fig. 5 is due to exciton-exciton spin exchange interaction. The temperature dependence and magnitude of the exchange broadening $W_{exch.}$ can be understood simply in terms of the following formula (13).

$$\sqrt{3}\,\pi\, W_{exch.} \simeq 2f\tau^{-1} C \exp(-V(2)/kT \tag{15}$$

Here f is the fraction of "close" spin exchange collisions that are effective in producing line broadening, and V(2) is the phonon-coupled repulsion between adjacent localized triplet excitons (18). By a "close" collision we mean one that surmounts the potential barrier V(2) so that the localized excitations are on nearest neighbor sites. It is very reasonable to assume that all close collisions are "strong pulse" (19) line broadening collisions, for which $f \sim 1$. This is because the exchange broadening interaction during a close encounter (J' in the notation of our previous paper (7)) is precisely the same interaction that gives rise to the exciton motion (7), so that $\tau^{-1} \sim J'$. On the other hand, $J'\tau \gtrsim 1$ is the condition for a "strong pulse" collision (19). Thus, $f \sim 1$. The observed temperature dependence of $W_{exch.}$ seen in Fig. 5, and in the earlier work of Jones and Chesnut (3), is ac-

counted for if $V(2) \lesssim J$. (To be more precise, for both the line width data of Jones and Chesnut (3), and ours in Fig. 5, a plot of line width vs. $C^{1.8}$ gives the best straight line. This corresponds to a $V(2) = 0.050$ ev. when $J = 0.065$ ev.)

An analysis of the data in Fig. 5, curve (a), in terms of Eq. (15) with $f \sim 1$, leads to an exciton jump rate τ^{-1} of the order of 10^{12} sec^{-1}. An analysis of similar high field data obtained by Jones and Chesnut leads to a τ^{-1} of the order of 10^{12} sec^{-1}. We note these estimated jumping frequencies are also in order-of-magnitude agreement with the jump rate obtained above in the discussion of nuclear hyperfine contributions to the line width. We conclude that an exciton diffusional motion with a jumping frequency of the order $\sim 10^{12}$ appears to account for the observed exciton resonance line widths in pure samples of $(\phi_3 AsCH_3)^+(TCNQ)_2^-$.

The data in Fig. 6 show that the broadening of the exciton resonance by a unit concentration of free radical impurity is of the order of 10^4 times less effective than the broadening of the exciton resonance by a unit concentration of the excitons themselves. The apparent constancy of the line broadening at exciton concentrations above $\sim 4 \times 10^{-3}$ due to the free radical impurity can be understood in terms of a formula similar to Eq. (15) in which the free radical contribution to the broadening is proportional to $f\tau^{-1} C_f$, where C_f is the free radical impurity concentration. In the present case where the free-radical broadening is of the order of 10^6 sec^{-1}, and $C_f \sim 10^{-2}$, $\tau^{-1} \sim 10^{12}$, f must be of the order of 10^{-4}, implying "weak pulse" collisions. The tailing off of the free radical contribution to the exciton line broadening below an exciton

concentration of $C \sim 4 \times 10^{-3}$ is not understood, but might be associated with a small barrier to exciton-free radical spin exchange collisions.

The foregoing discussion of line widths is obviously crude, incomplete, and tentative. On the other hand, exciton line widths clearly provide a key to an understanding of exciton motion in solid free radicals, and the foregoing estimates appear to be useful starting points for more comprehensive theoretical (20) and experimental studies.

References

1. See, for example, H. M. McConnell, D. Pooley and A. Bradbury, Proc. Natl. Acad. Sci. (U.S.) 48, 1480 (1962).
2. D. B. Chesnut and W. D. Phillips, J. Chem. Phys. 35, 1002 (1961).
3. M. T. Jones and D. B. Chesnut, J. Chem. Phys. 38, 1311 (1963).
4. H. M. McConnell, D. D. Thompson and R. W. Fessenden, Proc. Natl. Acad. Sci. (U.S.) 45, 1600 (1959).
5. T. Cole, T. Kushida and H. C. Heller, J. Chem. Phys. 38, 2915 (1963).
6. H. M. McConnell and R. M. Lynden-Bell, J. Chem. Phys. 36, 2393 (1962).
7. R. M. Lynden-Bell and H. M. McConnell, J. Chem. Phys. 37, 794 (1962).
8. R. G. Shulman, Phys. Rev. 121, 125 (1961).
9. R. C. LaForce, Rev. Sci. Inst. 32, 1387 (1961).
10. H. M. McConnell, H. O. Griffith, and D. Pooley, J. Chem. Phys. 36, 2518 (1962).
11. C. Dean and R. V. Pound, J. Chem. Phys. 20, 194 (1952).
12. See, for example, H. Bayer, Z. Physik 131, 227 (1951), and T. Kushida, G. B. Benedek, and N. Bloembergen, Phys. Rev. 104, 1364 (1956) and further references contained therein.
13. D. D. Thomas, H. Keller and H. M. McConnell, J. Chem. Phys. 39, 2321 (1963).
14. See, for example, T. T. Harding and S. C. Wallwork, Acta. Cryst. 8, 787 (1955) and N. D. Jones and R. E. Marsh, Acta Cryst. 15, 809 (1962).

15. The existence of this anisotropy was originally noted by D. Chesnut (private communication). The numerical values quoted here are from unpublished measurements of O. H. Griffith, H. Keller and H. M. McConnell.

16. In unpublished and incomplete work, O. H. Griffith, H. Keller and H. M. McConnell have noted a most remarkable similarity between the high-field, low-temperature (77°K) exciton line width anisotropy and the observed hyperfine line width anisotropy of free radical impurities in the $(\phi_3AsCH_3)^+(TCN_2)_2^-$ crystal. This suggests that the free radical impurity is $TCNQ^-$, that this radical has an orientation similar to that of the $(TCNQ)_2^-$ pairs on which the triplet excitons move, and that the exciton line width anisotropy does indeed arise from nuclear hyperfine interactions. Experiments with perdeutero TCNQ are in progress to test this conjecture.

17. Exceptions to this statement can arise if a significant number of zero-field nuclear hyperfine splittings are degenerate with the exciton fine structure splittings.

18. H. M. McConnell and Z. Soos, J. Chem. Phys. (in press).

19. H. M. McConnell and S. B. Berger, J. Chem. Phys. 27, 230 (1957); C. S. Johnson, Jr., J. Chem. Phys. 39, 2111 (1963).

20. A detailed theory of resonance line broadening due to exchange collisions between diffusing S = 1 excitons has been developed by R. M. Lynden-Bell, Mol. Phys. (in press).

Legends to Figures

Fig. 1. - Zero-field energy states. The spin Hamiltonian is

$$\mathcal{H} = XS_x^2 + YS_y^2 + ZS_z^2$$

Fig. 2. - Zero-field exciton magnetic resonance signals in $(\phi_3AsCH_3)^+(TCNQ)_2^-$ at 111°K. Line widths are measured at points of maximum slope.

Fig. 3. - The y-polarized transition in $(\phi_3AsCH_3)^+(TCNQ)_2^-$ at 96°K, 122°K, and 131°K.

Fig. 4. - Temperature dependence of x and y transition frequencies in pure and "dirty" samples of $(\phi_3AsCH_3)^+(TCNQ)_2^-$ in zero field. The shift of the resonance frequency in the "dirty" sample relative to the pure sample is attributed to a second-order exchange interaction between excitons and spin 1/2 free radical impurities in the "dirty" sample.

Fig. 5. - Relation between zero-field line widths in $(\phi_3AsCH_3)^+(TCNQ)_2^-$ and exciton concentration. Curve (a) gives line widths for the y-polarized transition (squares, □) and x-polarized transitions (circles, ○) in pure sample I (see text), and curve (b) gives line widths for the y-polarized transition in "dirty" sample II (see text).

Legends to Figures (cont'd)

Fig. 6. - Calculated free radical contribution to the exciton line width in the "dirty" sample containing ca. 1% free radical spin 1/2 impurities. The broadening is attributed to exchange interaction between excitons and the spin 1/2 free radical impurities.

Fig. 7. - Exciton dimer spectrum. When two excitons are coupled by a weak time independent exchange interaction, J_{eff}, the zero-field absorption at ν_y is split by first-order exchange interaction into three equally strong lines at $\nu_y - J_{eff}$, ν_y and $\nu_y + J_{eff}$. The shift of the outer lines to higher frequencies by second order exchange is shown by the dotted lines.

Fig. 8. - Model used for the calculation of the temperature dependence of the zero-field transition frequencies due to molecular torsional motion. Two coaxial benzene negative ions with uniform spin density oscillate through an angle θ relative to each other.

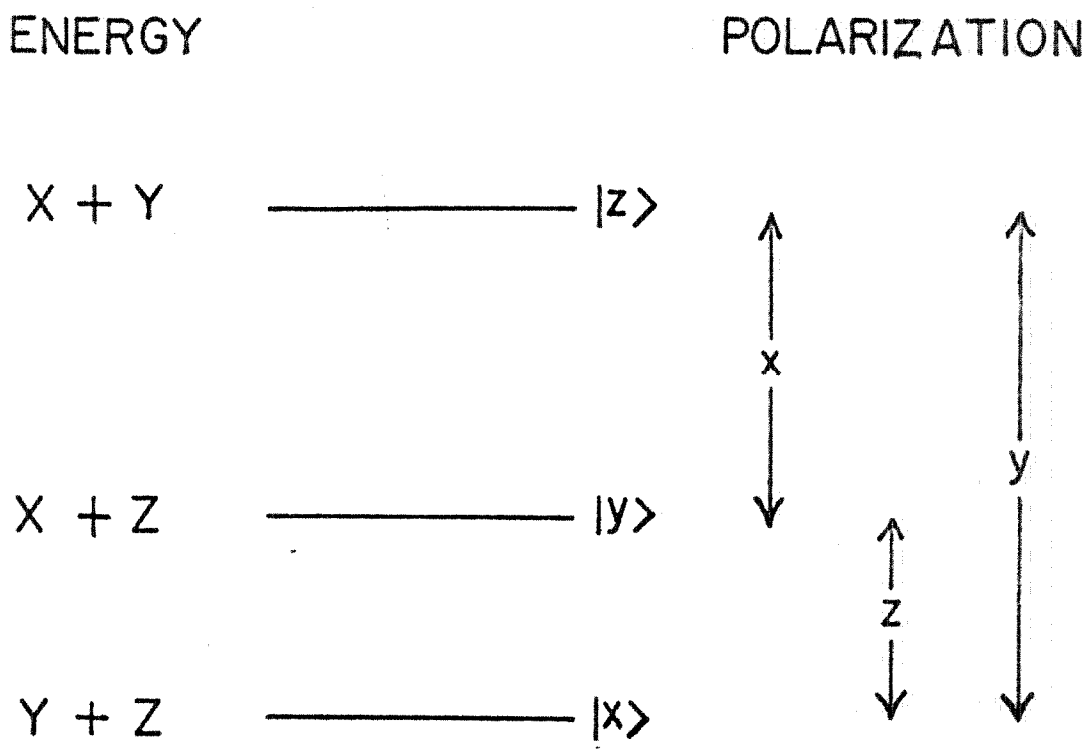
ENERGY
POLARIZATION
X + Y
|z>
X + Z
|y>
Y + Z
|x>
x
y
z

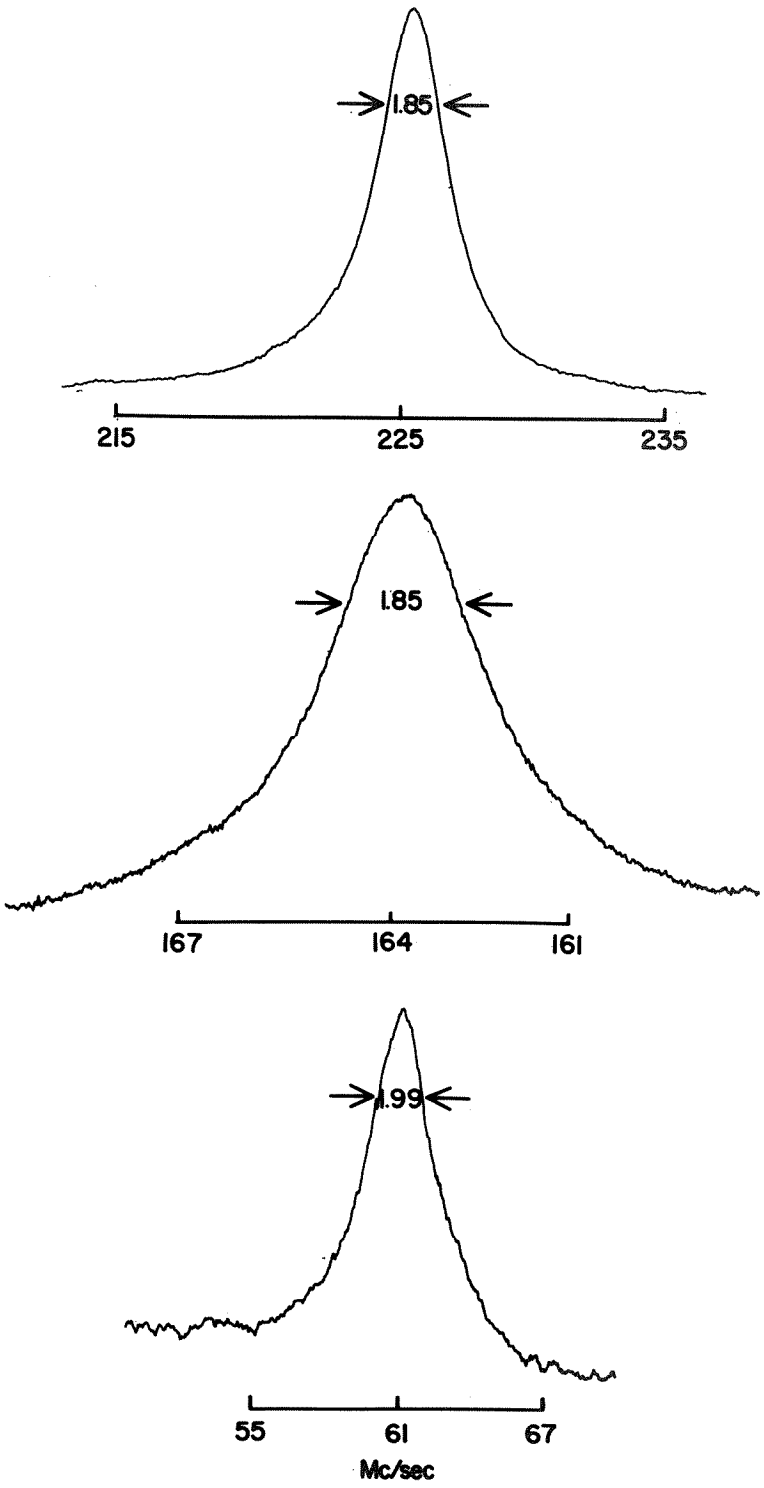
1.85
215
225
235
1.85
167
164
161
1.99
55
61
67
Mc/sec

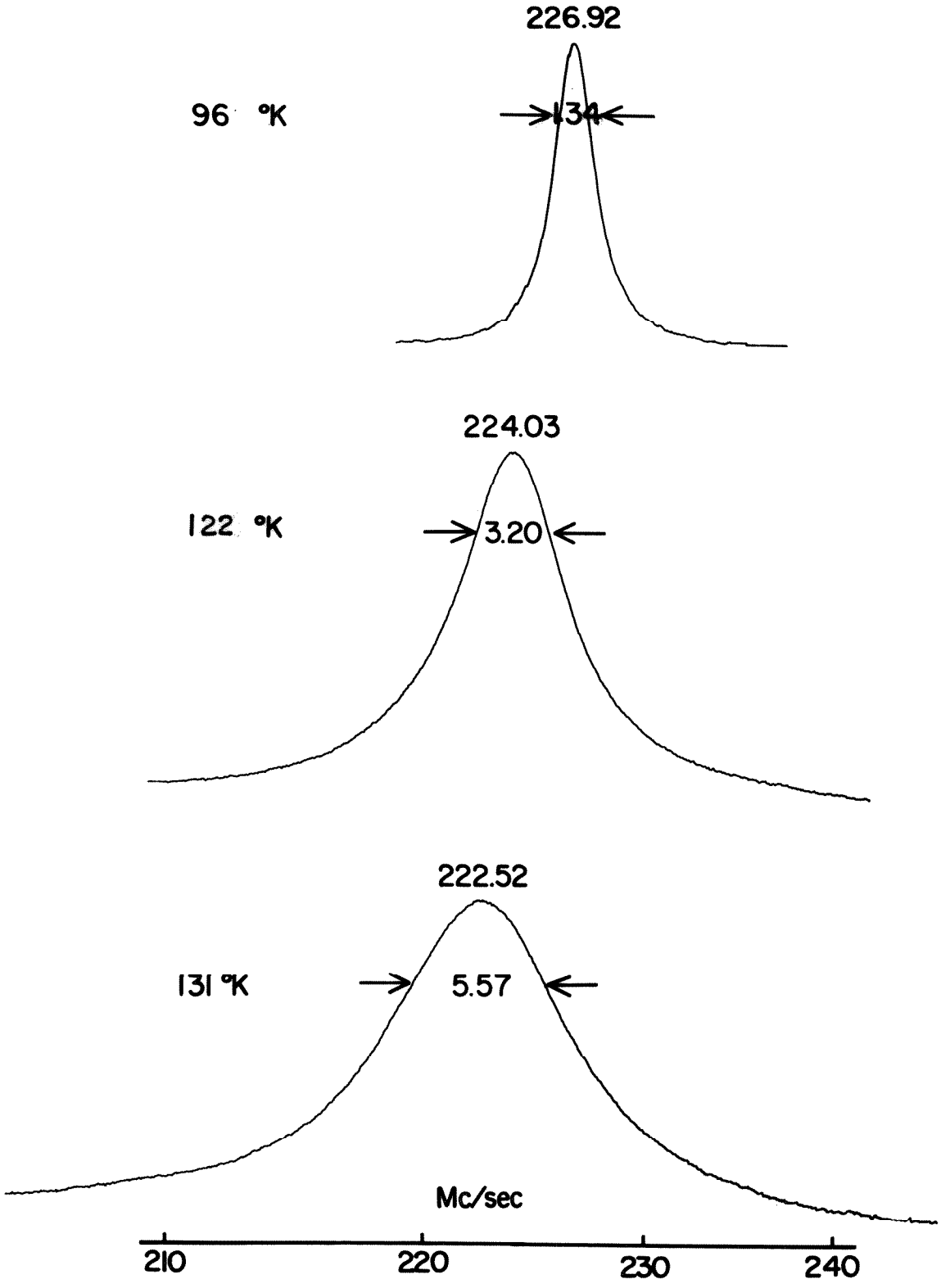
226.92
96 °K
1.34
224.03
122 °K
3.20
222.52
131 °K
5.57
Mc/sec
210
220
230
240

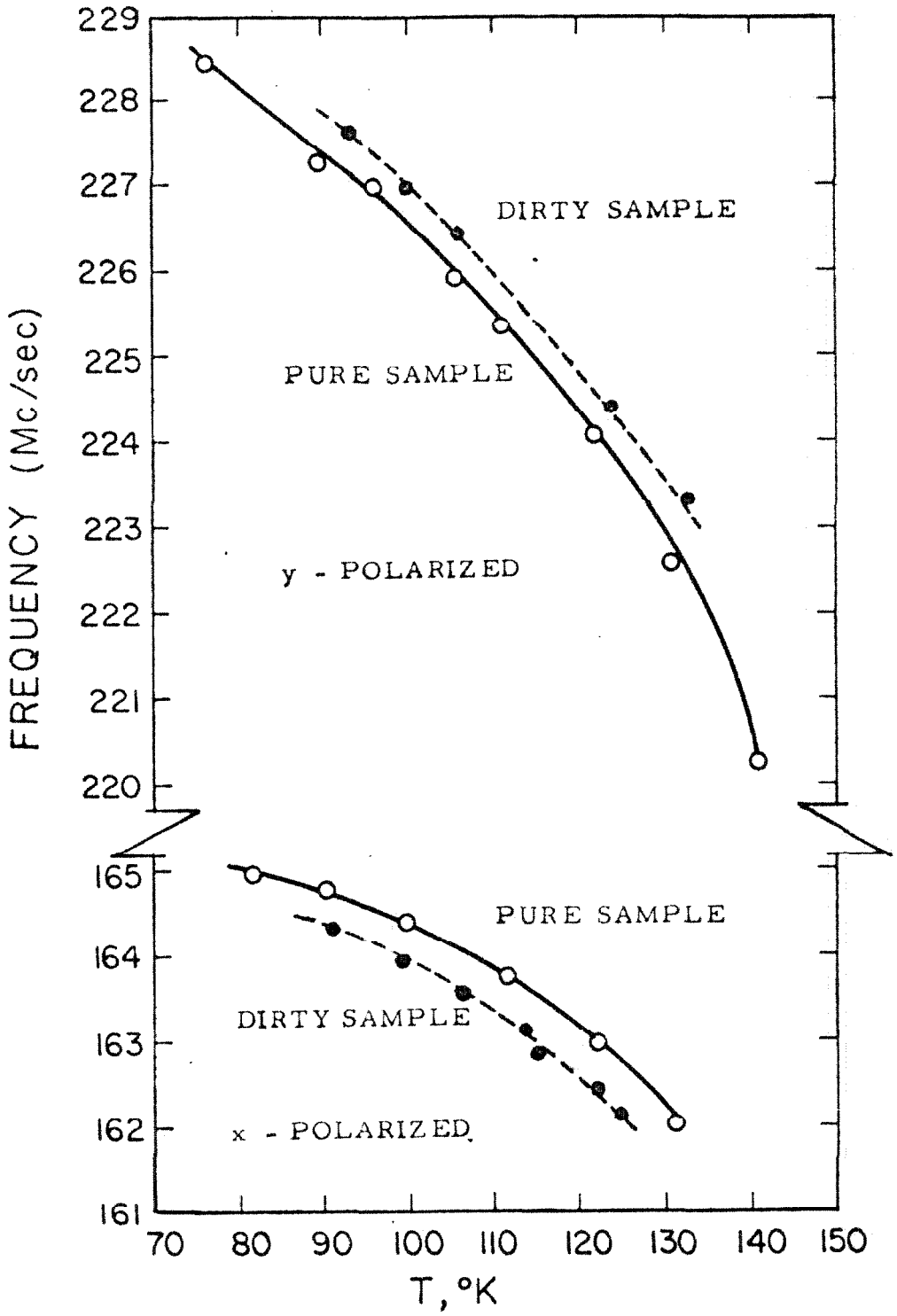
229
228
227
226
225
224
223
222
221
220
165
164
163
162
161
FREQUENCY (Mc/sec)
DIRTY SAMPLE
PURE SAMPLE
y - POLARIZED
PURE SAMPLE
DIRTY SAMPLE
x - POLARIZED
70
80
90
100
110
120
130
140
150
T, °K

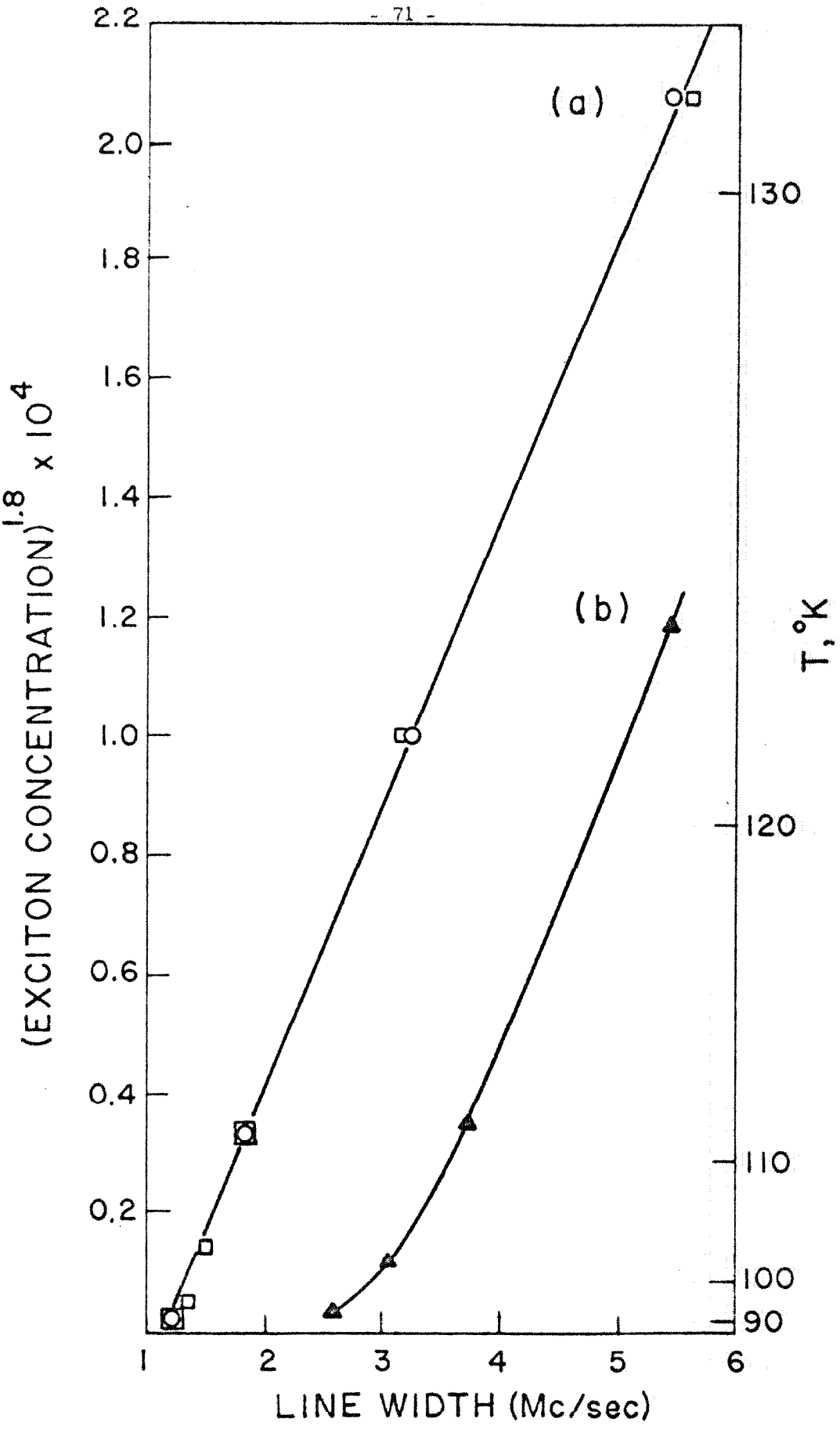
(a)
(b)
2.2
2.0
1.8
1.6
1.4
1.2
1.0
0.8
0.6
0.4
0.2
(EXCITON CONCENTRATION)^1.8 x 10^4
130
120
110
100
90
T, °K
1
2
3
4
5
6
LINE WIDTH (Mc/sec)

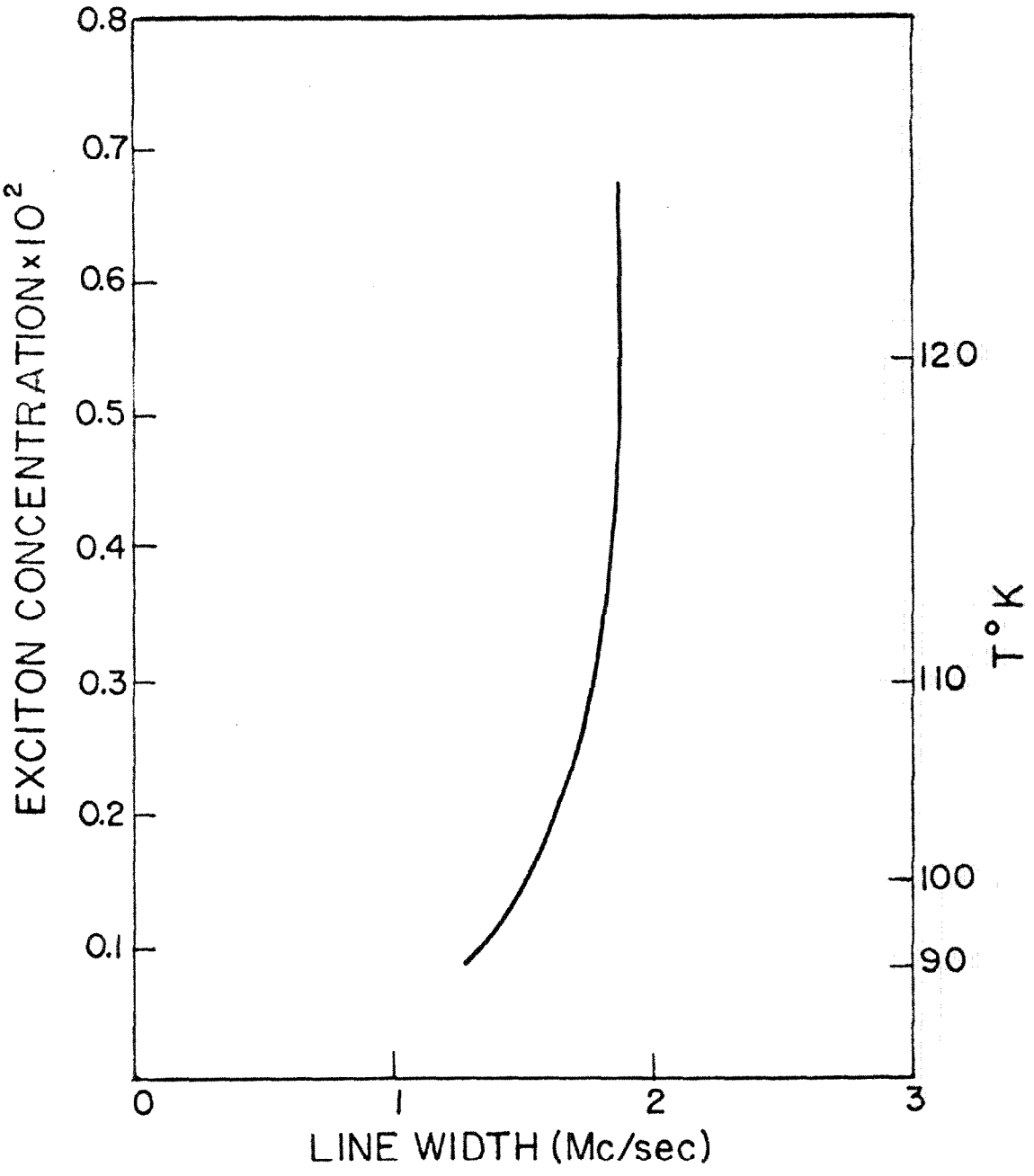
0.8
0.7
0.6
0.5
0.4
0.3
0.2
0.1
EXCITON CONCENTRATION×10²
120
110
100
90
T°K
0
1
2
3
LINE WIDTH (Mc/sec)

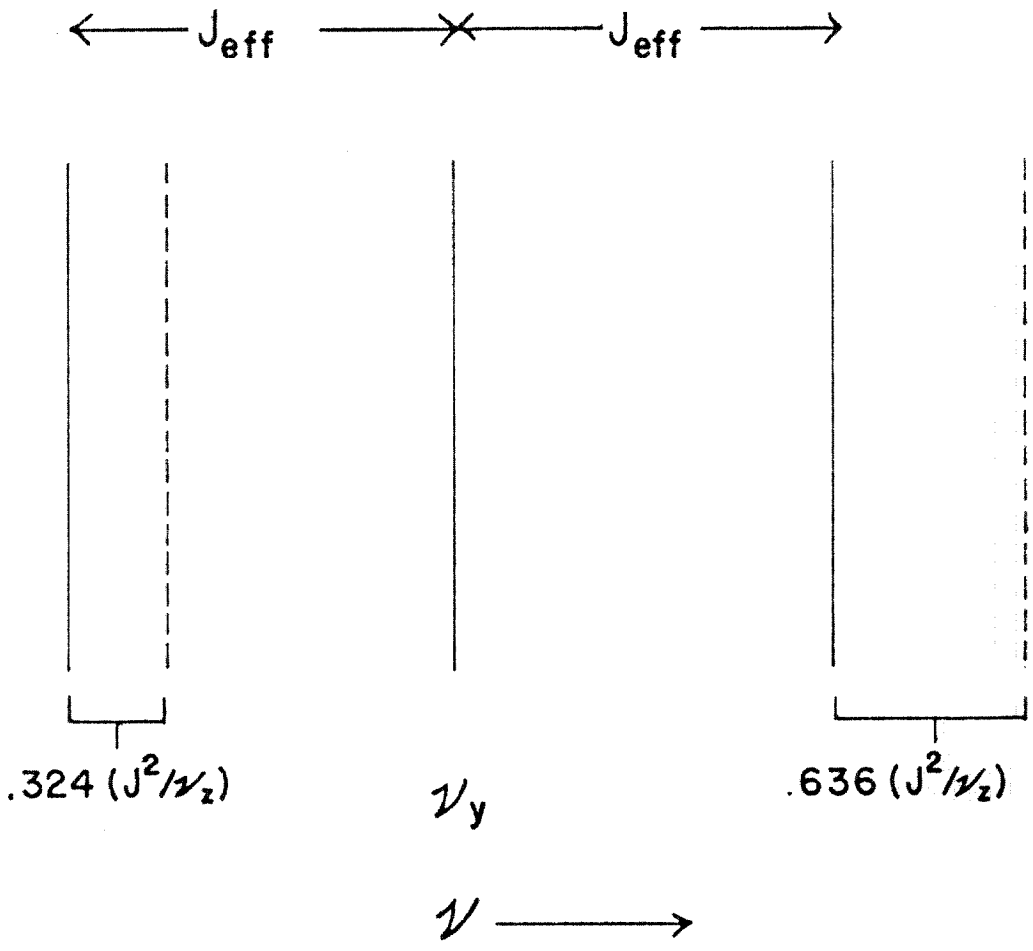
J_{eff}
J_{eff}
$.324\,(J^2/\nu_z)$
ν_y
$.636\,(J^2/\nu_z)$
ν

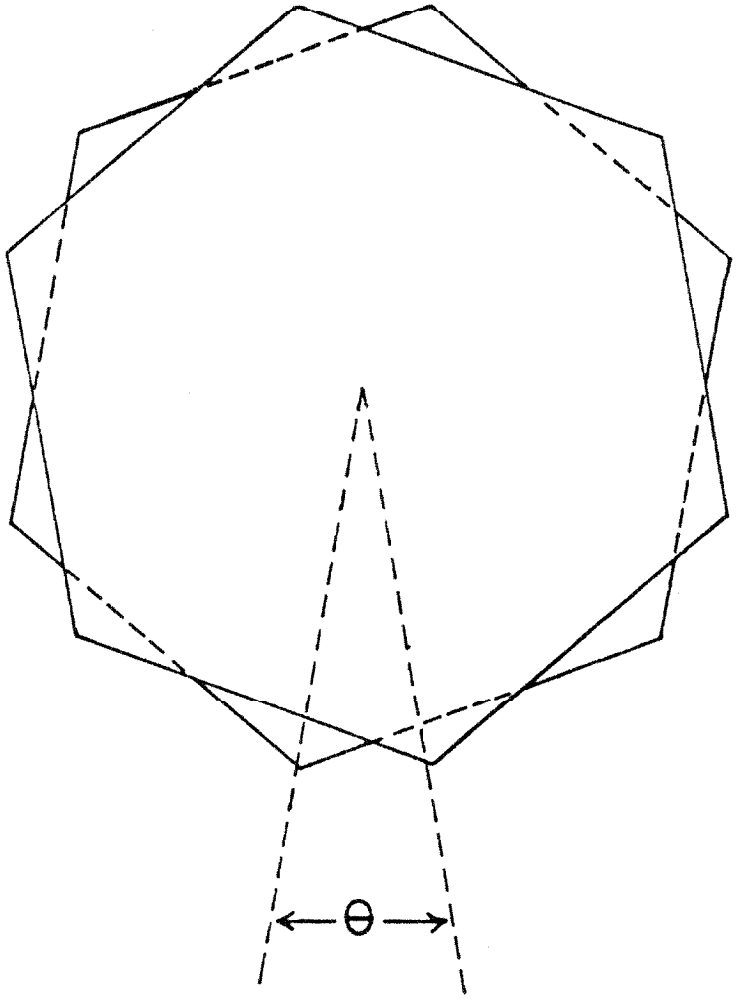
θ

PART II

A ZERO FIELD MAGNETIC RESONANCE SPECTROMETER

Operation of the Spectrometer

Figure 8 gives a block diagram of the spectrometer used in the 60 Mc/sec zero field study of triplet excitons in the (Ø AsCH) (TCNQ) radical salt system (see section I-E). The useable frequency range is 10 - 100 megacycles/sec.

The radio frequency energy needed for the zero field transitions is provided by the RF marginal oscillator for which figure 9 is a schematic diagram. The oscillator is almost identical to the one built by H. R. Moore and H. Hopper (42). The wide band amplifier used was a Hewlett-Packard Model 460A. As will be explained later, best results could be obtained when this amplifier was replaced with a short piece of coaxial cable. The frequency was measured using a Hewlett-Packard Model 524C frequency counter and a Model 525A plug-in unit.

The frequency is swept by rotating the butterfly capacitor in the "tank circuit" with a variable speed motor. When the point of resonance is reached the level of oscillation will be decreased due to the absorption of energy by the sample. This change in level is detected by the 1N100 diode in the detector circuit and if this change occurs at an alternating rate, e.g., the modulation frequency, the signal will be amplified by the preamplifier.

The oscillator circuit also contains an automatic level control (ALC). Any small variations in the RF level due to frequency dependent variations in the oscillator are compensated for by the ALC. The

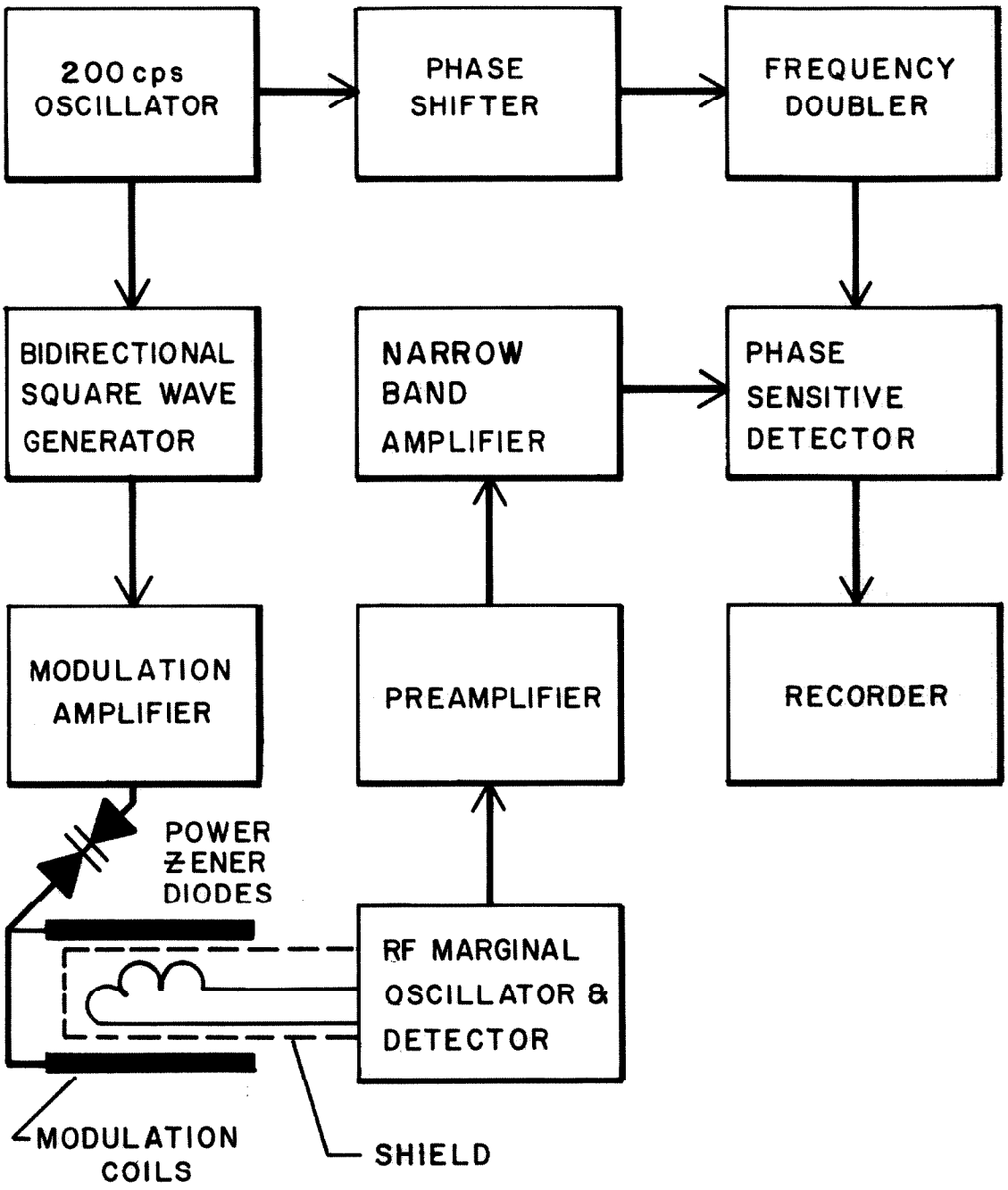

Figure 8. Block diagram of zero field spectrometer

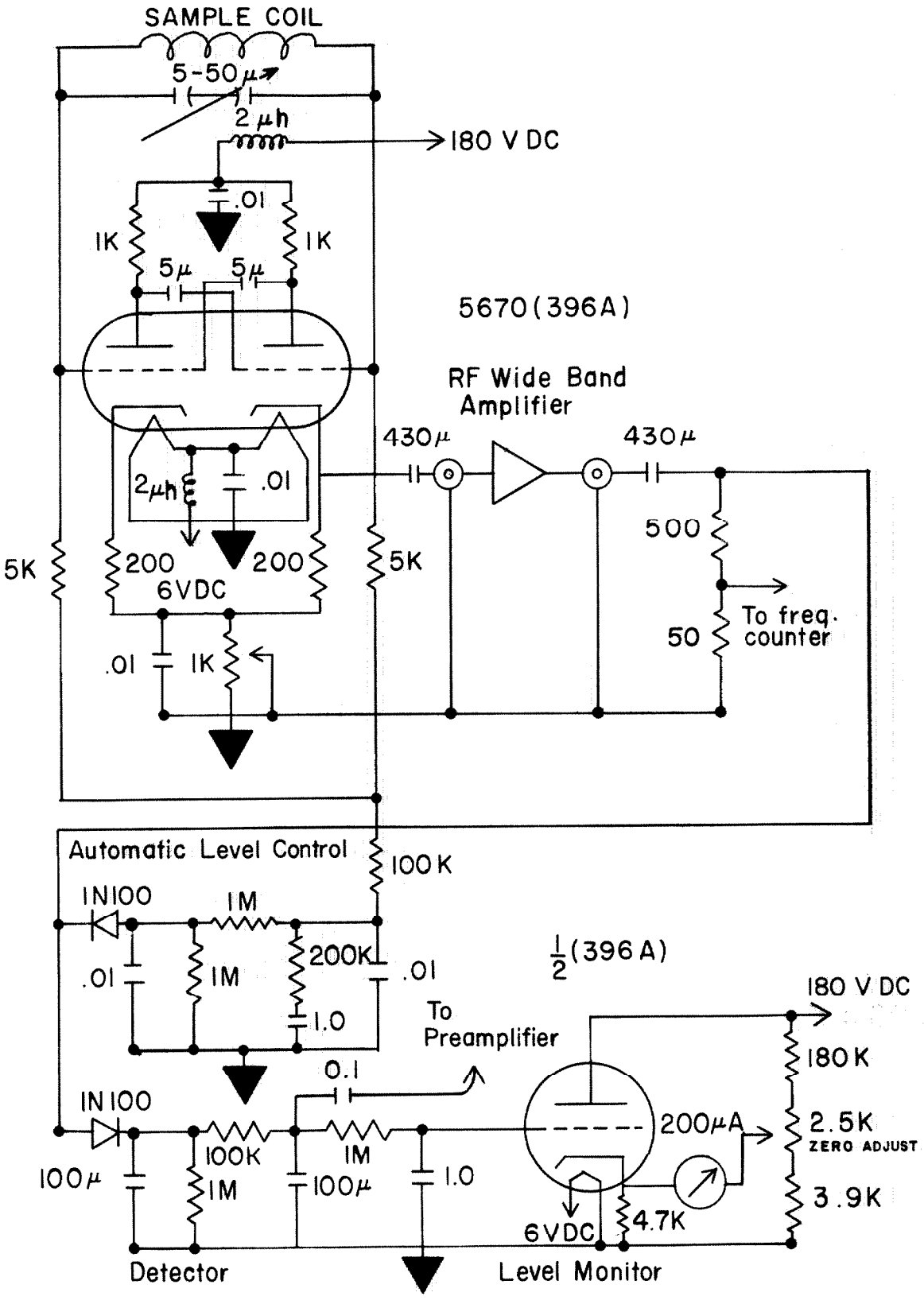

Figure 9. RF marginal oscillator. Capacitance is expressed in microfarads.

ALC has a one second time constant and therefore will not effect the level changes due to a resonance signal at the modulation frequency. The oscillation level can be adjusted by varying the cathode bias with the 1K potentiometer in the cathode circuit. This level is constantly monitored by means of a DC follower after the detector.

A schematic diagram of the preamplifier is shown in figure 10. This unit has a gain of 250 and a low noise level.

The narrow band amplifier used is a Pickard and Burns, Inc. Model 60 bolometer amplifier. The initial input transformer in the amplifier is bypassed in order to fit the present application.

Figure 11 shows a schematic diagram of the phase sensitive detector and recorder output control. The reference signal of a 10 volt RMS 400 cps sine wave is supplied by the frequency doubler (see below). The time constant is determined by the capacitance switched across the level control. An analysis of the circuit shows that the magnitude of the time constant is equal to the capacitance times 200K ohm resistance. A differential output to the recorder is provided by the 12AU7 DC follower circuit. Any constant DC level is compensated for by the balance control. A Brown Potentiometer strip chart recorder is used to record the spectra.

Principal of Bidirectional Square Wave Modulation

When a DC magnetic field is applied to a powder sample of a paramagnetic material in zero field, in general the energy levels

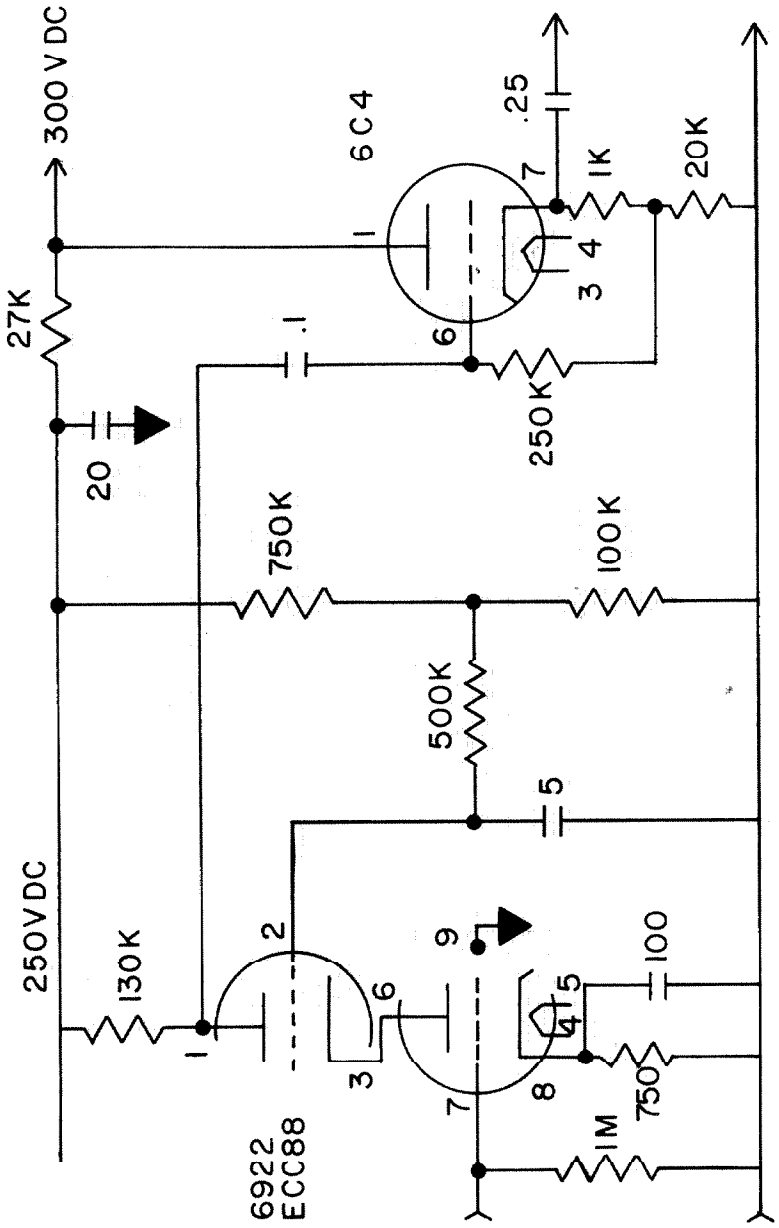

Figure 10. Preamplifier. Capacitance is expressed in microfarads.

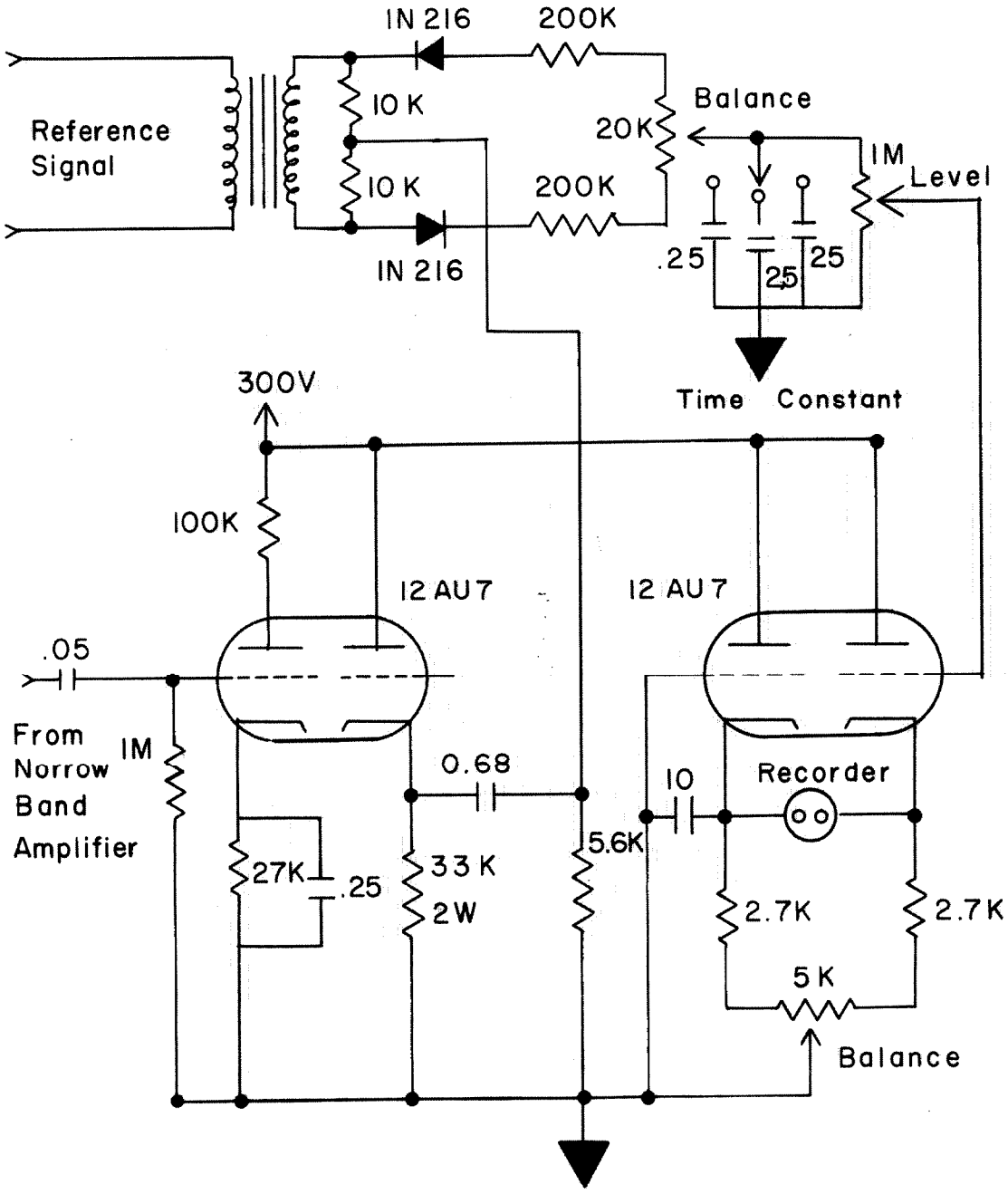

Figure 11. Phase sensitive detector. Capacitance is expressed in microfarads.

become broad and shift in frequency. If a marginal oscillator such as the one described above is set at a zero field transition energy of a paramagnetic sample and a DC magnetic field is turned on and off at a given rate, the level of oscillation will change at the same rate. When the field is on, the level of the oscillator will be the same as if no sample were present. When the field is off, the sample absorbs energy and the level of oscillation deminishes. Thus if the field has the form of a square wave, i.e. on for 1/2 cycle, off 1/2 cycle, etc., there will be a square wave superimposed on the RF level of the oscillator.

Furthermore, if the field is of the form of a bidirectional square wave, i.e. on (-) for 1/4 cycle, off for 1/4 cycle, on (+) for 1/4 cycle, off for 1/4 cycle, etc., there are certain advantages. Let the fundamental frequency of the bidirectional square wave be f_o, i.e. f_o equals the inverse of the time between two adjacent positive pulses. Since the field effect on the sample is the same regardless of the direction of the field, the oscillation level will change at the rate of $2f_o$. An analysis of the bidirectional square wave itself however, will show that only frequencies f_o, $3f_o$, $5f_o$, etc. are contained herein. Therefore any magnetic pickup in the system caused directly from the bidirectional square wave modulation will not be amplified by the narrow band amplifier, which only amplifies at the signal frequency, $2f_o$.

Since the change in the oscillator level is proportional to the

absorption of energy in the sample, the amplitude of the signal at $2f_o$ is proportional to the absorption of energy. The phase sensitive detector measures the amplitude of the $2f_o$ signal and, thus, the recorder plots the actual absorption curve vs. frequency. The following discussion explains the electronic methods used in producing this bidirectional square wave and $2f_o$ reference signal for the phase sensitive detector.

For the present spectrometer f_o was chosen to be 200 cps. The reasons for this choice are several. A 400 cps narrow band amplifier was available in the lab. Also the higher the modulation frequency the greater is the magnetic pick up in different components in the oscillator circuit. It is also increasingly harder to make "sharp" corners in the bidirectional wave form at higher frequencies due to the inductances of the modulation coil and the output transformer of the modulation amplifier.

The 200 cps audio oscillator feds the bidirectional wave form generator shown in figure 12. Here the signal is divided and goes to two separate circuits, one producing the positive pulse and the other one the negative pulse. The final stage then combines these outputs, thus synthesizing the bidirectional square wave. The initial stage of each circuit contains a potentiometer, a 1N457 diode and a 1N732 56 volt zener diode. This part of the circuit allows only the peak part of the sine wave to appear across the 22K resistor. In the upper

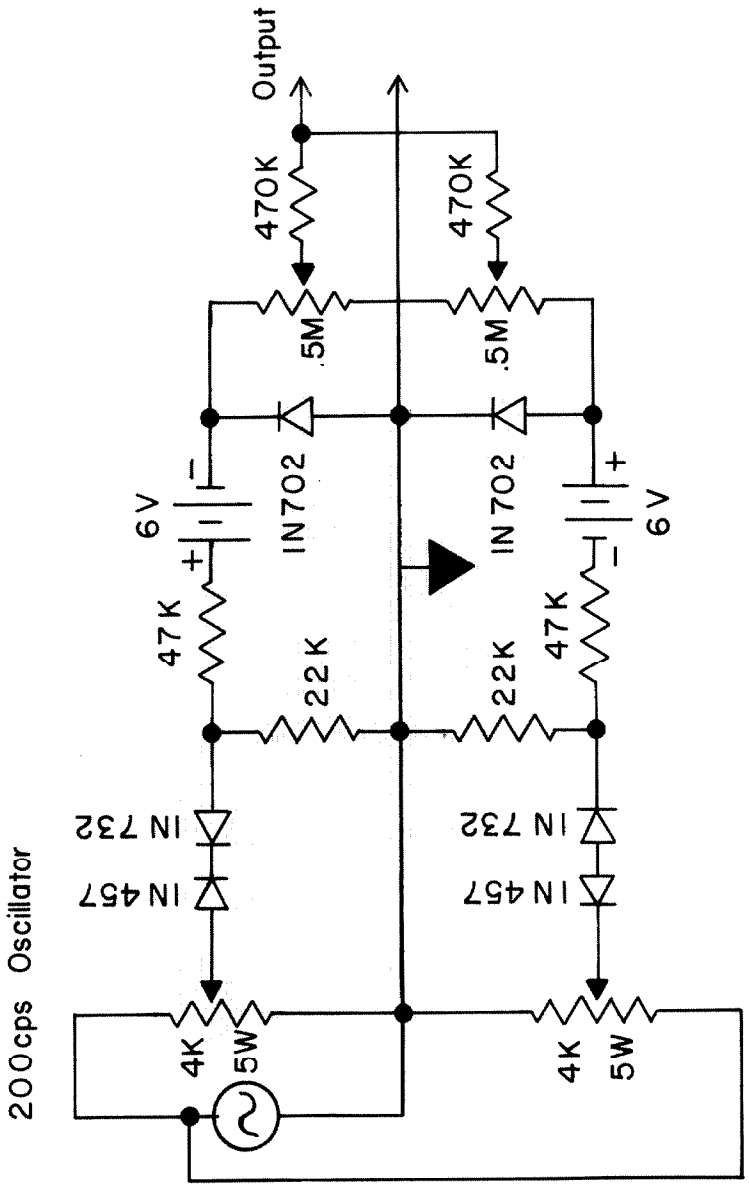

Figure 12. Bidirectional wave form generator.

circuit, for example, until the voltage at the potentiometer tap reaches + 56 volts (relative to ground) no voltage will appear across the 22K resistor. The voltage across the load resistor will then follow the upper part of the sine wave until the voltage again drops to +56 volts. On the negative voltage swing, current will not flow because of the 1N457 diode. Thus a series of positive voltage humps is obtained. The analysis of the lower circuit is identical except negative pulses 180^{o} out of phase are obtained.

The width of these humps can be varied both by changing the voltage of the audio oscillator (normally run at about 180 volts peak to peak) and changing the voltage tapped off at the potentiometer. The former adjustment will vary the width of both the positive and negative pulses simultaneously, and the latter adjustment will vary the width of the positive and negative pulses independently.

The next part of the circuit consists of a current limiting resistor, a 6 volt battery and a 1N702 2.6 volt zener diode. This part of the circuit is used to "clip off" the upper part of the voltage hump. Were the 1N732 a perfect zener diode, i.e., turn on and off very sharply, the 6 volt battery would not be needed. In practice, however, there is a certain amount of tailing off after the voltage across the 1N732 has dropped below 56 volts. In order to dispose of these tails, a 6 volt battery is placed in the next stage. Under these circumstances the 1N702 2.6 volt zener diodes will clip the voltage hump above

(or below) 8.6 volts and a voltage will appear across the 1N702's only when the voltage across the 22K resistor is plus (or minus) 6 volts or greater. Thus there is a series of 2.6 volt positive (or negative) pulses across the 1N702's.

In the final stage these negative and positive pulses are added together to give the bidirectional square wave. The .5 meg potentiometers are used to independently vary the height of the positive and negative pulses. A high percentage of isolation between the upper and lower circuits is achieved by use of the 470K resistors to the output.

Overall the above circuit produces a very useable bidirectional square wave form. Since only a very small section of the input sine wave is used (2.6 volts out of 90 volts), a fairly good vertical slope on the pulses is achieved. In practice it is found that the inductance of the modulation coils limit the steepness of the pulse slopes more than the above circuit.

During the later experiments this bidirectional wave form generator was replaced by one Tektronix Model 162 Wave form generator and two Model 161 pulse generators.

From the bidirectional square wave generator the modulation signal goes to the modulation amplifier. A Heathkit Model W-6A 70 watt hi-fi amplifier provides the modulation power. Inserted between the amplifier and the modulation coils are two 1N2804 6.8 volt 50 watt zener diodes mounted back to back. The purpose of these diodes is to prevent any small voltage fluctuations during the off part of the

cycle producing a field at the sample. The power zener diodes also help in keeping the corners of the modulation wave form square.

The modulation coils are wound in the form of Helmboltz coils 3 inches in diameter. There are about 100 turns of wire on each coil and the two coils are wired in parallel. The axis of the modulation coils is perpendicular to the axis of the RF coil in order to minimize the amount of direct audio pickup by the sample coil.

A 200 cps signal also goes to the phase shifter shown in figure 13. The purpose of the phase shifter is to compensate for any phase shifts in any of the components of the spectrometer. Thus the reference signal to the phase sensitive detector is always completely in phase (or 180^{o} out of phase) with any resonance signal coming from the narrow band amplifier.

The circuit used in doubling the frequency of the phase shifter signal is shown in figure 14. Basically it consists of a full wave rectifier followed by a narrow band amplifier tuned to 400 cps. The level is adjusted by the 10K input potentiometer. Two pairs of matched 1N34's are used in the full wave bridge rectifier. The narrow band amplifier uses a two stage amplifier with negative feedback in the second stage. The feedback loop consists of a null T network which has a null frequency of 400 cps. This circuit is very adequate in producing the necessary $2f_o$ reference signal.

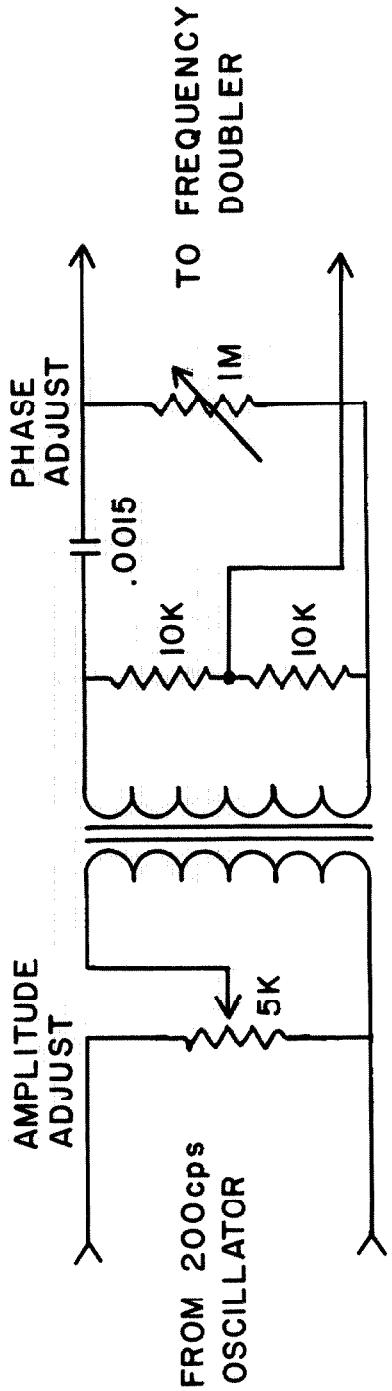

Figure 13. Phase shifter. Capacitance is expressed in microfarads.

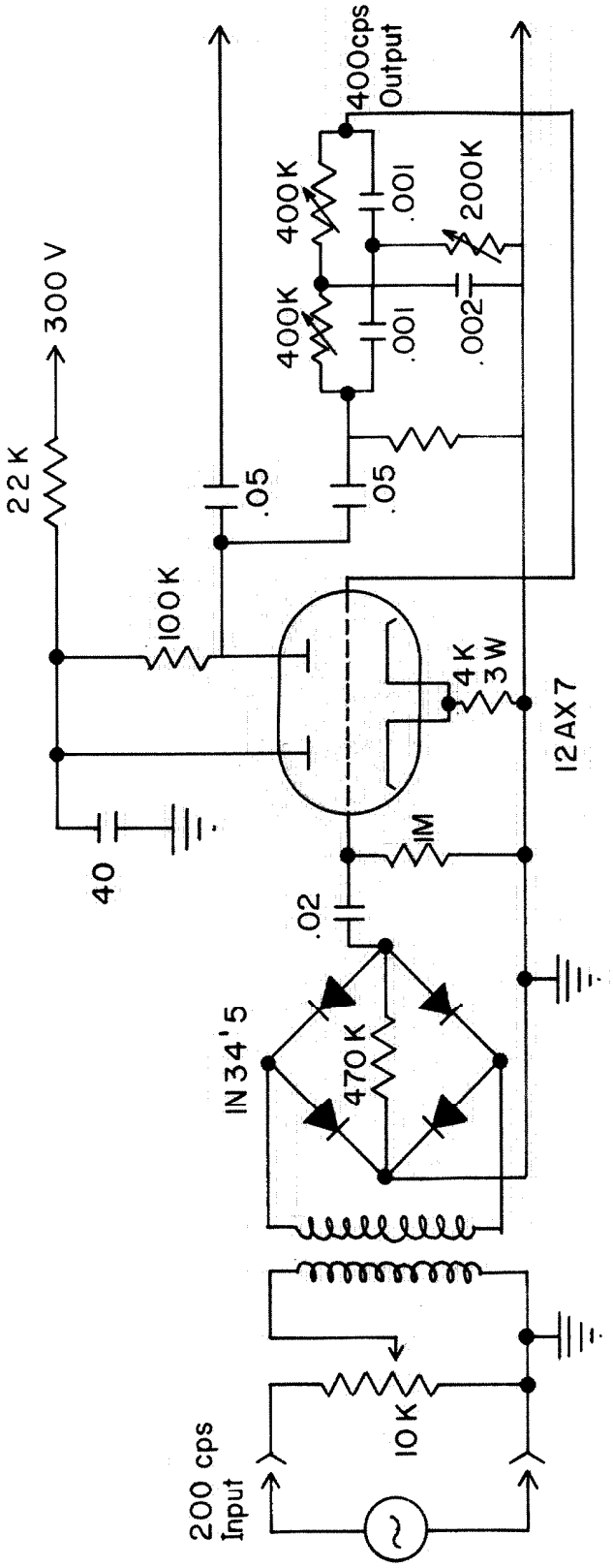

Figure 14. Frequency doubler (200 cps to 400 cps).
Capacitance is expressed in microfarads.

Construction of the Spectrometer

Although most of the individual components of the spectrometer were made in the laboratory, the only part of the spectrometer that required special construction practices was the radio frequency marginal oscillator. The present discussion will therefore be limited to the construction of the oscillator.

Since the oscillator is of the push-pull design, extreme care was taken in the symetrical placement of the part of the two sides. All resistors used had a 1% tolerance. A symmetrical butterfly capacitor was used in the tank circuit. Due to the relatively high frequency range of the oscillator, leads were kept as short as possible. The circuit in figure 9 was built in a partitioned one-fourth inch thick brass box made specifically for this application. The main RF circuit of the oscillator was constructed in one section of the box, and all leads (with the exception of the sample coil) entered this section through feed through capacitors. All external connectors where of the BNC type.

As mentioned above best results were obtained when the RF wide band amplifier was not used. Although the oscillator appeared to be more stable when wide band was used, the amount of 60 cycle noise introduced by this amplifier due to B plus ripple and pickup more than off set and advantages of the unit. Moreover, the oscillator did work satisfactorily when the wide band amplifier was not used.

The major trouble encountered in making the spectrometer

operational was the problem of modulation pickup. The largest single source of pickup was found to be capacitive pickup between the modulation coils and the sample coil. This source of pickup was eliminated by shielding the sample coil with two half cylinders three inches in diameter of aluminum foil grounded to the oscillator chasis. Two separate halves were used rather than one complete cylinder in order to minimize any eddy currents produced by the modulation field.

Many of the individual components in the oscillator circuit were found to be quite sensitive to modulation magnetic field. Paper electrolytic capacitors were particularly sensitive, and these capacitors were replaced by the small tantalum type. A two foot by two foot 1/2" aluminum plate was placed between the modulation coils and the oscillator chasis, and in this way the modulation field was further reduced. With the above construction practices and the use of bidirectional square wave modulation (with the pickup at frequencies f_o, $3f_o$, $5f_o$, etc., and the signal at $2f_o$) a satisfactory system was found.

References

1. H. M. McConnell and R. M. Lynden-Bell, J. Chem. Phys. 36, 2393 (1962).

2. R. M. Lynden-Bell, and H. M. Mc Connell, J. Chem. Phys. 37, 794 (1962).

3. H. Sternlicht and H. M. McConnell, J. Chem. Phys. 35, 1793 (1961).

4. D. B. Chesnut and W. D. Phillips, J. Chem. Phys 35, 1002 (1961).

5. D. B. Chesnut and P. Arthur, Jr., J. Chem. Phys. 36, 2969 (1962).

6. H. M. McConnell, D. Pooley, and A. Bradbury, Proc. Nat. Acad. Sci. U. S. 48, 1480 (1962).

7. K. W. H. Stevens, Proc. Roy. Soc. (London) A214, 237 (1952).

8. H. J. Silverstone, private communication.

9. J. H. Van Vleck, Phys. Rev 74, 1168 (1948).

10. C. P. Slichter, Principles of Magnetic Resonance, (Harper and Pow, 1963), p. 54.

11. S. I. Weissman, J. Chem. Phys. 22, 1135, (1954).

12. T. R. Tuttle, J. Chem. Phys. 30, 331 (1959).

13. K. H. Hausser, Z. Naturforsh 14A, 425 (1959).

14. K. H. Hausser, Naturwiss. 47, 251 (1959).

15. J. R. Bolton, A. Carrington, and J. dos Santos-Veiga, Mol. Phys. 5, 615 (1962).

16. T. L. Chu, G. E. Pake, D. E. Paul, J. Townsend, and S. I. Weissman, J. Phys. Chem. 57, 504 (1953).

17. A. S. Edelstein and M. Mandel, J. Chem. Phys. 35, 1130 (1961).

18. R. S. Rhodes, J. H. Burgess, and A. S. Edelstein, Phys. Rev. Letters 6, 462 (1961).

19. N. Elliot and M. Wolfsberg, Phys. Rev. 91, 435 (1955).

20. W. Duffy, Jr., J. Chem. Phys. 36, 490 (1962).

21. K. H. Hausser, Z. Naturforsch. 11a, 20 (1956).

22. K. H. Hausser and H. Kainer, Chem. Ber. 86, 1563 (1953).

23. Clear exciton paramagnetic resonance spectra of polycrystalline samples of WB perchlorate at 50°K were observed in this laboratory.

24. J. D. Turner and A. C. Albrecht, unpublished work. The work has not been published due to some uncertainties in the orientation of the perchlorate ions.

25. R. E. Peierls, Quantum Theory of Solids, (Oxford University Press, 1956) P. 108.

26. H. C. Longuet-Higgins and L. Salem, Proc. Roy. Soc. (London) A251, 172 (1959).

27. Y. Ooshida, J. Phys. Soc. Japan, 12, 1238, 1246 (1957); 14, 747 (1949).

28. C. Montgomery and H. M. McConnell, unpublished.

29. R. Lynden-Bell and H. M. McConnell, unpublished.

30. Still earlier discussion of dimerization have been given by G. K. Hughes and N. S. Hersh, J. Proc. Roy. Soc., N. S. Wales 81, 48 (1947), and by L. Michaelis and S. Granick, J. Am. Chem. Soc. 65, 1747 (1943).

31. K. H. Hausser and J. N. Murell, J. Chem. Phys. 27, 500 (1957).

32. A method similar to that of Michaelis and Granick was used. See reference (30).

33. M. T. Jones and D. B. Chesnut, J. Chem. Phys. 38, 1311 (1963).

34. G. E. Pake and T. R. Tuttle, Jr., Phys. Rev. Letters 3, 423 (1959).

35. H. Sternlicht, Thesis, California Institute of Technology, Pasadena, 1962.

36. C. A. Hutchison and B. W. Mangum, J. Chem. Phys. 29, 952 (1958); 34, 908 (1961).

37. J. H. van der Waals and M. S. deGroot, Mol. Phys. 2, 333 (1959); 3, 190 (1960).

38. H. M. McConnell, J. Chem. Phys. 28, 1188 (1958).

39. A. D. McLachlan, Mol. Phys. 1, 233 (1958).

40. H. M. McConnell, H. O. Griffith, and D. Pooley, J. Chem. Phys. 36, 2518 (1962).

41. H. M. McConnell and Z. Soos, J. Chem. Phys. (in press).

42. R. G. Shulman, Phys. Rev. 121, 12 (1961).

Proposition No. 1

The ability to vary the sample temperature between $4^{o}K$ and room temperature in much zero field electron magnetic resonance work is of extreme importance. In the frequency range from 10 to 100 megacycles per second there are several factors which contribute to the difficulty of this problem. The sample must be placed in the coil of the "tank circuit" of the radio frequency oscillator. Since this coil is typically about one-half to one inch in diameter, the conventional cold finger Dewar consisting of one or two vacuum jackets is too bulky to fit inside the sample coil and still leave room for a large sample. Thus, using the conventional cold finger Dewar, the maximum available filling factor is quite small.

The sample coil cannot be lowered into the center chamber of a conventional Dewar since the leads between the sample coil and the remainder of the radio frequency oscillator must be kept as short as possible (6 inches or less). If these leads are made too long, the upper frequency limit of the oscillator is reduced, the sensitivity of the oscillator is reduced and the frequency sweeping ability of the oscillator is reduced.

A proposed Dewar design for use in the temperature range approximately $4^{o}K$ to room temperature is given in figure P1 - 1. The Dewar would be constructed out of pyrex with the exception of the most central cylinder which would be made out of quartz. The sample

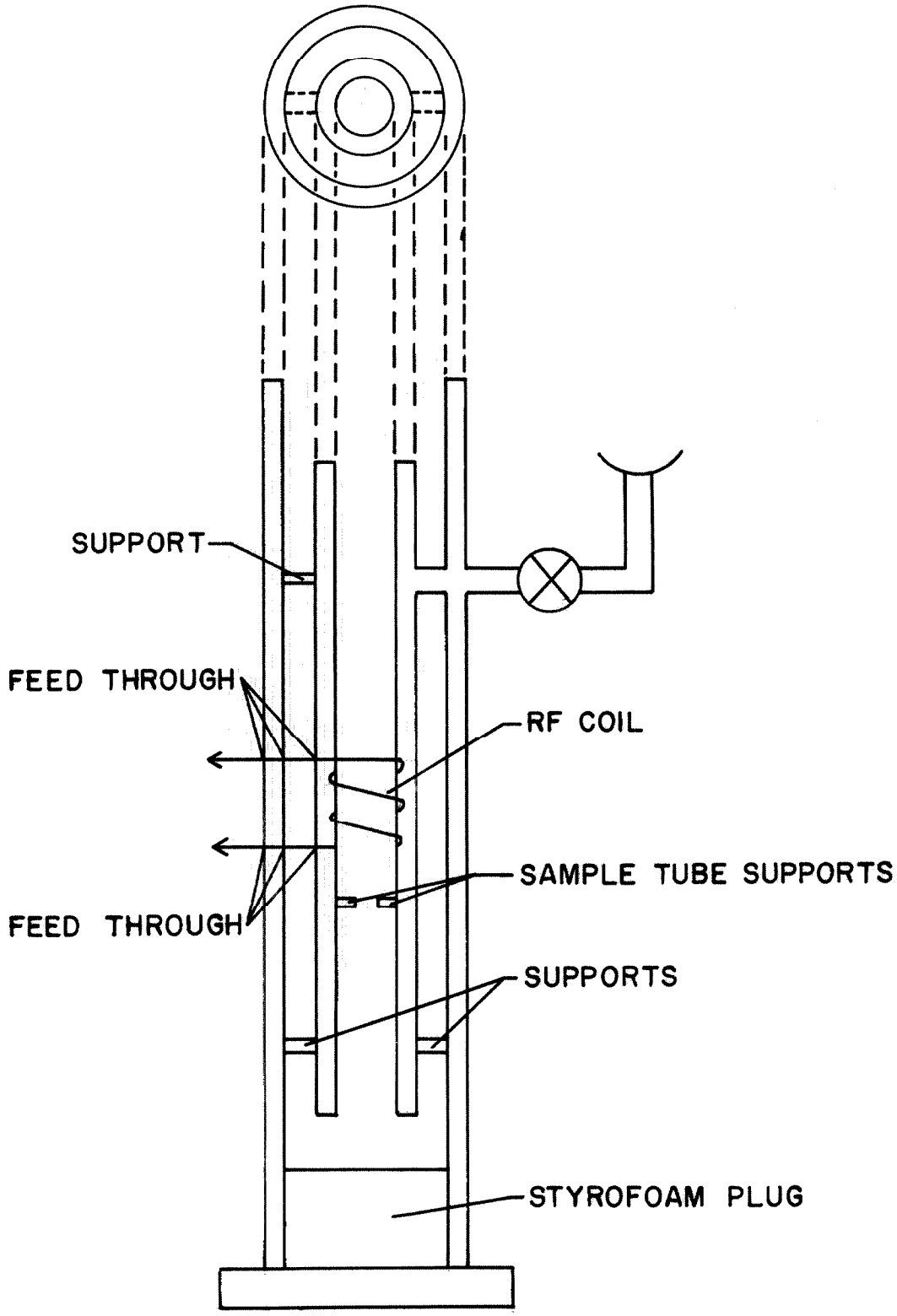

Figure P1 -1. Dewar designed for use in zero field magnetic resonance work.

would be placed in an etched quartz tube and supported in the Dewar by the sample tube supports.

The sample coil would be wound around the center quartz tube and held in place by several small poor-heat-conducting supports such as polystyrene or micarta. The leads from the sample coil would be brought directly through the remaining glass walls. These feed throughs could be either small diameter platinum wire encased in the glass or perhaps copper wire epoxied in small holes previously drilled through the glass walls.

Cold nitrogen or helium gas at the appropriate temperature would enter the center chamber, flow around the sample and out the outside chamber. The cold gas flowing in the outside chamber serves two purposes. First it provides a radiation shield for the inside chamber, and second it cools the feed throughs of the sample coil, thus minimizing the "heat leak" caused by the sample coil leads.

Proposition No. 2

Recently there has been some debate as to the sign of the nitrogen-hyperfine coupling constant in the ESR spectra of heterocyclic anions. Using the theory of Stephen and Fraenkel (1) and Schreurs (2), Henning and Waard (3) and Carrington (4) concluded from their experiments that the signs of the nitrogen coupling constant for the case where the spin density is on the atom adjacent to the nitrogen atom are both positive. This result is in contradiction to Karplus and Fraenkel's theory (5) from which it follows that these two coupling constants should have opposite signs.

In a high magnetic field, the sign of the coupling constants can only be determined from second order effects such as the line widths (1) (2). In zero field, however, it can be shown that the relative signs of the nitrogen coupling constant and the proton coupling constant, in a free radical where the electron interacts with one nitrogen nucleus and one proton, can be determined from the direct measurement of the transition frequencies.

In zero magnetic field the spin Hamiltonian for a free radical undergoing rapid tumbling and one in which the electron interacts with one nitrogen and one proton is given by

$$\mathcal{H} = a_N I_N \cdot S + a_H I_H \cdot S \qquad \text{(P2-1)}$$

where a_N and a_H are the nitrogen and proton hyperfine coupling constants, respectively, and I_N, I_H and S are the nitrogen, proton and

electron spin operators, respectively. Equation (P2-1) may also be expressed in the following form

$$\mathcal{H} = \frac{a_N}{2}(I_{N-}S_+ + I_{N+}S_- + 2I_{N_z}S_z) + \frac{a_H}{2}(I_{H-}S_+ + I_{H+}S_- + 2I_{H_z}S_z) \qquad \text{(P2-2)}$$

where the + and − refer to the spin raising and lowering operators respectively.

Using the following basis states,

$$\begin{aligned} \phi_1 &= |1, \alpha, \alpha\rangle & \phi_7 &= |0, \beta, \alpha\rangle \\ \phi_2 &= |1, \alpha, \beta\rangle & \phi_8 &= |0, \beta, \beta\rangle \\ \phi_3 &= |1, \beta, \alpha\rangle & \phi_9 &= |-1, \alpha, \alpha\rangle \\ \phi_4 &= |1, \beta, \beta\rangle & \phi_{10} &= |-1, \alpha, \beta\rangle \\ \phi_5 &= |0, \alpha, \alpha\rangle & \phi_{11} &= |-1, \beta, \alpha\rangle \\ \phi_6 &= |0, \alpha, \beta\rangle & \phi_{12} &= |-1, \beta, \beta\rangle \end{aligned} \qquad \text{(P2-3)}$$

where the number refers to the nitrogen spin state, the first α or β refers to the proton spin state, and the final α or β refers to the electron spin state, the resulting 12 by 12 energy matrix can be further subdivided into the following energy matrices,

$$\begin{array}{c} \\ \phi_1 \\ \phi_{12} \end{array} \begin{array}{c} \begin{array}{cc} \phi_1 & \phi_{12} \end{array} \\ \begin{pmatrix} \frac{a_N}{2} + \frac{a_H}{4} & 0 \\ 0 & \frac{a_N}{2} + \frac{a_H}{4} \end{pmatrix} \end{array}$$

$$
\begin{array}{c} \\ \phi_{11} \\ \phi_{10} \\ \phi_{8} \end{array}
\begin{array}{c}
\begin{array}{ccc} \phi_{11} & \phi_{10} & \phi_{8} \end{array} \\
\begin{pmatrix}
-\frac{a_N}{2}-\frac{a_H}{4} & \frac{a_H}{2} & \frac{a_N}{\sqrt{2}} \\
\frac{a_H}{2} & \frac{a_N}{2}-\frac{a_H}{4} & 0 \\
\frac{a_N}{\sqrt{2}} & 0 & \frac{a_H}{4}
\end{pmatrix}
\end{array}
$$

$$
\begin{array}{c} \\ \phi_{2} \\ \phi_{3} \\ \phi_{5} \end{array}
\begin{array}{c}
\begin{array}{ccc} \phi_{2} & \phi_{3} & \phi_{5} \end{array} \\
\begin{pmatrix}
-\frac{a_N}{2}-\frac{a_H}{4} & \frac{a_H}{2} & \frac{a_N}{\sqrt{2}} \\
\frac{a_H}{2} & \frac{a_N}{2}-\frac{a_H}{4} & 0 \\
\frac{a_N}{\sqrt{2}} & 0 & \frac{a_H}{4}
\end{pmatrix}
\end{array}
$$

$$
\begin{array}{c} \\ \phi_{4} \\ \phi_{7} \\ \phi_{6} \\ \phi_{9} \end{array}
\begin{array}{c}
\begin{array}{cccc} \phi_{4} & \phi_{7} & \phi_{6} & \phi_{9} \end{array} \\
\begin{pmatrix}
-\frac{a_N}{2}+\frac{a_H}{4} & \frac{a_N}{\sqrt{2}} & 0 & 0 \\
\frac{a_N}{\sqrt{2}} & -\frac{a_H}{4} & \frac{a_H}{2} & 0 \\
0 & \frac{a_H}{2} & -\frac{a_H}{4} & \frac{a_N}{\sqrt{2}} \\
0 & 0 & \frac{a_N}{\sqrt{2}} & -\frac{a_N}{2}+\frac{a_H}{4}
\end{pmatrix}
\end{array}
$$

Solving the above matrices the following energies are found:

Level	Degeneracy	Energy	
E_1	4	$\frac{a_H}{4} + \frac{a_N}{4}$	(P2-5)
E_2	2	$-\frac{a_H}{4} - \frac{a_N}{4} + \frac{1}{2}(a_H^2 - a_H a_N + \frac{9}{4}a_N^2)^{1/2}$	
E_3	2	$-\frac{a_H}{4} - \frac{a_N}{4} - \frac{1}{2}(a_H^2 - a_H a_N + \frac{9}{4}a_N^2)^{1/2}$	
E_4	1	$\frac{a_H}{4} - \frac{a_N}{2}$	
E_5	1	$-\frac{a_H}{12} - \frac{a_N}{6} + A + B$	
E_6	1	$-\frac{a_H}{12} - \frac{a_N}{6} - \frac{A+B}{2} + \frac{A-B}{2}\sqrt{-3}$	
E_7	1	$-\frac{a_H}{12} - \frac{a_N}{6} - \frac{A+B}{2} - \frac{A-B}{2}\sqrt{-3}$	

where

$$A = \Big[-.03704a_H^3 + .02777a_H^2a_N + .09722a_Ha_N^2 - .08796a_N^3 + (-.02083a_H^4a_N^2 + .02546a_H^3a_N^3 - .04225a_H^2a_N^4 + .00463a_Ha_N^5 - .03935a_N^6)^{1/2}\Big]^{1/3}$$

and

$$B = \Big[-.03704a_H^3 + .02777a_H^2a_N + .09722a_Ha_N^2 - .08796a_N^3 - (-.02083a_H^4a_N^2 + .02546a_H^3a_N^3 - .04225a_H^2a_N^4 + .00463a_Ha_N^5 - .03935a_N^6)^{1/2}\Big]^{1/3}$$

As can be seen from an inspection of the above energies, the magnitude of the transition frequency between many of the levels is dependent on the relative signs of a_N and a_H. Thus, the magnitude of a_N and a_H can be determined in a high field experiment and with this information the relative sign of a_N and a_H could be determined.

References

1. M. J. Stephen and G. K. Fraenkel, J. Chem. Phys. 32, 1435 (1960).

2. J. W. Schreurs, Thesis, Vrije Universiteit, Amsterdam (1962).

3. J. C. M. Henning and C. De Waard, Phys. Letters 3, 139 (1962).

4. A. Carrington and H. C. Longuet - Higgins, Mol. Phys. 5, 447 (1962).

5. M. Karplus and G. K. Fraenkel, J. Chem. Phys. 35, 1312 (1961).

Proposition No. 3

There are several reports in the literature of dewar designs for the use in low temperature x-ray work (1). However, no dewar design has been reported that will work down to $4^{o}K$ and be adaptable to a commercially available Weissenberg camera. As was mentioned in section D of this thesis, the knowledge of the crystal structure as a function of temperature of free radicals exhibiting triplet excitons is extremely important. A proposed design for this type of dewar is given in figure P3-1.

The dewar with the goniometer and crystal inside enters the camera from the end opposite the spindle on the normal Weissenberg camera. Rotation of the goniometer and crystal is accomplished by the use of two concentric cylindrical magnets and a set of gears. As the spindle rotates this motion is transmitted to the magnet on the outside of the dewar by a series of gears and a shaft. The inner magnet, to which is attached the goniometer and crystal, follows the motion of the outside magnet. This method of rotation through a vacuum chamber has been used by Gerber (2). The inner magnet and assembly are supported by two sets of stainless steel ball bearings, which in turn are attached to the inside chamber of the dewar by stainless steel supports.

The crystal is kept at the desired temperature through the heat conduction of the crystal support which is made out of a good heat conductor such as teflon. This crystal support is in direct contact with

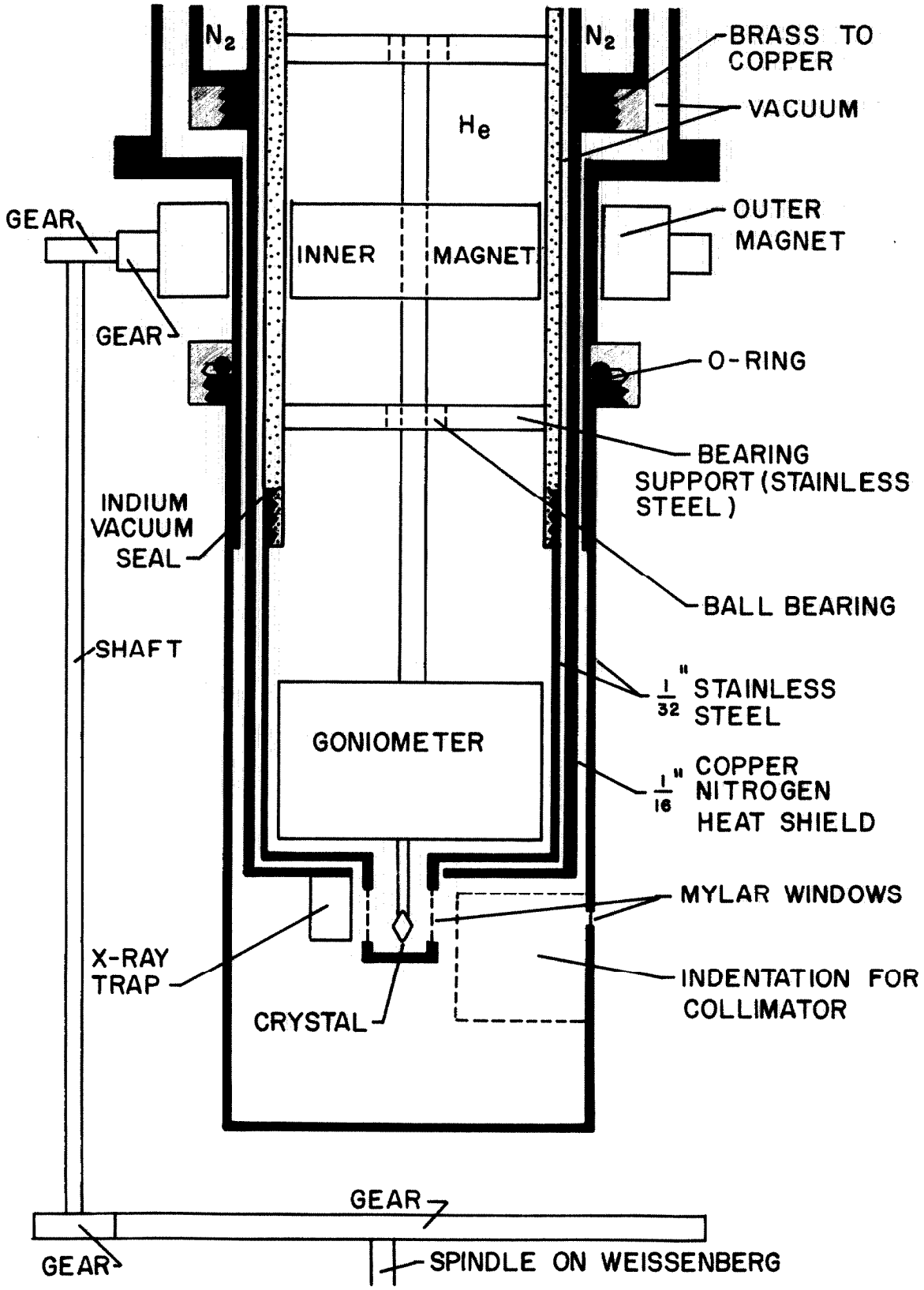

Figure P3-1. Proposed dewar design for use with Weissenberg x-ray camera.

the goniometer which is in contact with the cooling gas or liquid.

Movement of the layer line screen is accomplished by unscrewing the ring holding the o-ring seal and sliding it along the outside can of the dewar and then retightening the ring. Figure P3-1 also shows the position of the x-ray trap.

Since the cans at the bottom of the dewar are removeable, the crystals can be lined up at room temperature, the cans replaced and the dewar then cooled. Thus there are no problems of crystal alignment with the crystal in the dewar.

While the inside of the dewar is large enough to accommodate commercial goniometers, the outside of the dewar is too large to fit into the normal sized camera. However, a camera of slightly larger radius can easily be constructed.

To minimize construction difficulties, the dewar should be used in a vertical position. Therefore the Weissenberg camera would have to be mounted on a vertical rather than a horizontal plane. This procedure should present no difficulties, however.

References

1. C. A. Stochl and S. G. Ullman, Rev. Sci. Inst. 34, 1134 (1963) and references cited therein.

2. J. F. Gerber, Rev. Sci. Inst. 34, 1111 (1963).

Proposition No. 4

Cohen, Snow and Tretola have recently studied the temperature effects on a GaAs p-n junction diode (1). They have found that the forward voltage drop, at constant forward current, of this diode varies almost linearly with temperature from 2.0°K to above 300°K. The sensitivity of this device varies from about -1.5 mV/°C at 4°K to about -3.5mV/°C at room temperature, This diode can very easily be used in a temperature controlling device in the temperature range 4°K to room temperature.

In ESR work many studies require the temperature of the sample to be in the above range and to vary this temperature as well as to hold it at a given value. Figure P4-1 gives a schematic diagram of a system which would accomplish the above mentioned control.

The temperature of the sample is varied by varying the amount of cold gas cooling the sample (either He or N_2 depending on the temperature range). The gas flow rate is determined by the heat dissipated in the resistor immersed in the liquid.

The diode is placed near the sample. The current through the diode is provided by the 30 volt battery and adjusted by the 400K variable resistor. The rather large voltage is used so that small changes in the voltage drop of the diode will not seriously effect the current flow through the diode. (The voltage drop across the diode varies from about 0.5 volt to 1.5 volts depending on the temperature of the diode.)

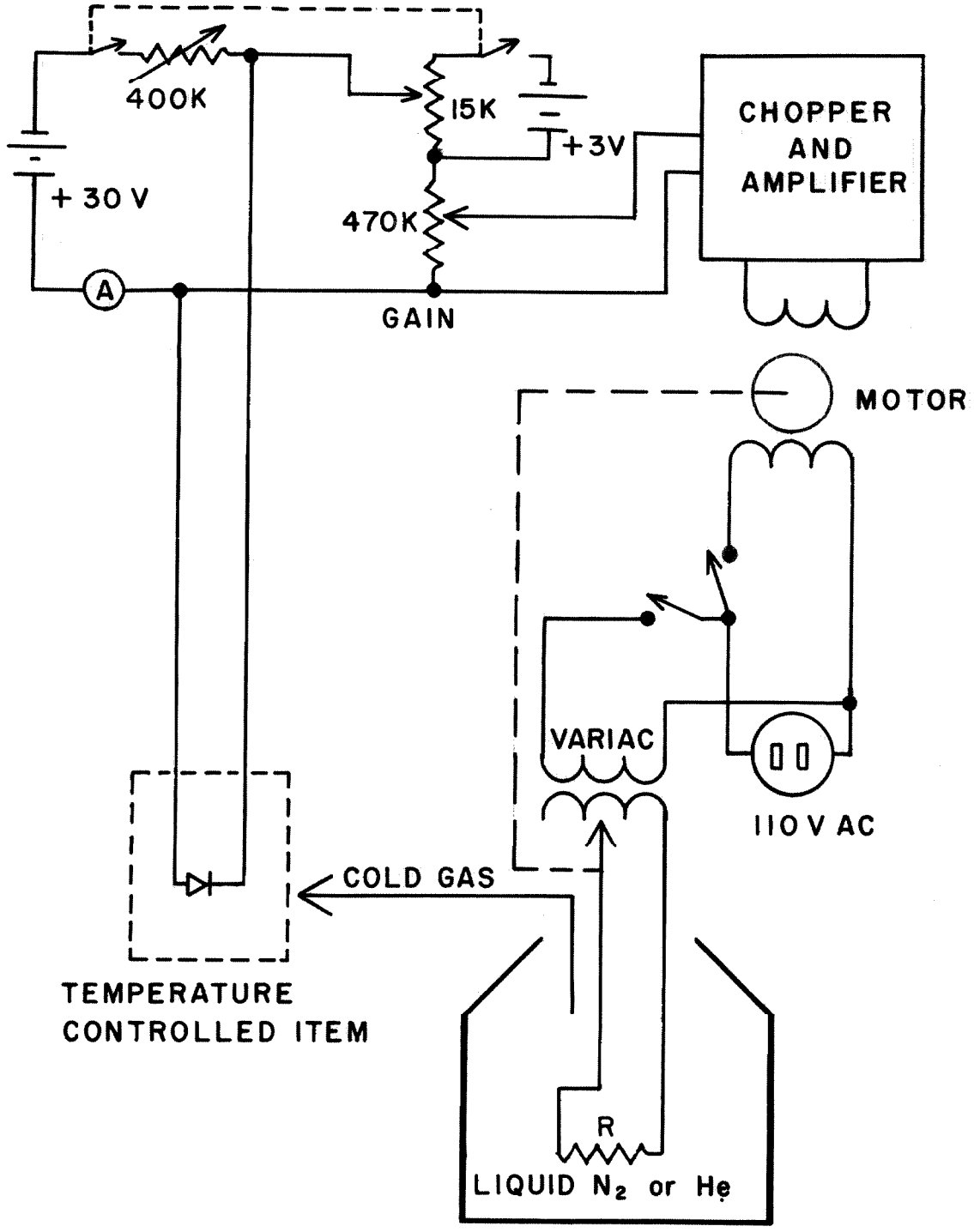

Figure P4-1. Proposed temperature controlling device for use in the 2 to 300°K temperature range.

The voltage across the diode is added to the voltage across the lower portion of the 15K potentiometer. This latter voltage is determined by the position of the center tap of the potentiometer. The resultant voltage is fed to a chopper and amplifier (similar to the chopper and amplifier found in strip chart recorders). The servo motor is then rotated in a direction dependent upon the sign of the above resultant voltage. The motor is attached to a Variac and the amount of current flowing through the resistor R is changed.

Thus once the voltage versus temperature curve for the diode is determined, the temperature of the sample can be regulated by adjusting the center tap on the 15K potentiometer to correspond to a voltage equal to the voltage of the diode at the desired temperature. If the diode is not at this desired temperature a resultant voltage will appear across the chopper and the motor will turn the Variac control until the proper gas flow rate is achieved to keep the sample at the proper temperature. At this point there will be no resulting voltage across the chopper and the motor will stop.

In order to prevent a large "over shoot" in temperature due to the thermal lag of the apparatus, a proper gear ratio must be used in the connection between the motor and Variac control to provide a "time constant". This gear ratio will be determined by the heat capacity of the system to be cooled.

Reference

1. B. G. Cohen, W. B. Snow, and A. R. Tretola, Rev. Sci. Inst. 34, 1091 (1963).

Proposition No. 5

Woodbrey and Rogers have reported on a study of the solvent effects on the hindered internal rotation about the C-N bond of two N, N-disubstituted amides - - N, N-dimethylpropionamide (DMP) and N, N-dimethylcarbamyl chloride (DMCC) (1). The NMR spectra of N, N-dimethylamides show a proton doublet corresponding to the two methyl groups. Phillips has shown this doublet to be the result of hindered rotation about the C-N bond (2). When the mean lifetime of rotation is sufficiently long, a doublet results from the different chemical shifts of the two sites. It was found that as the temperature was increased the two peaks broadened and became one (3). From this spectra the authors calculated the mean lifetime τ of rotation, and from the temperature dependence on τ calculated the energy barrier.

The authors made a study of the rotational energy barriers of the above two amides in solutions of CCl_4 and CH_2Br_2 at several concentrations. They found the following results. The rotational energy barrier, E_a, decreased monotonically with dilution with CCl_4 in both the DMP-CCl_4 and DMCC-CCl_4 systems. E_a for DMP varied from 9 kcal/mole at100% amide to 6 kcal/mole at 10% amide, while E_a for DMCC varied from about 7.3 kcal/mole to about 6.7 kcal/mole over the same range of concentration. When CH_2Br_2 was used as a solvent, however, E_a for both DMP and DMCC first increased with dilution to a maximum at about 60 mole percent amide and then de-

creased to the same value found in the CCl_4 systems at large dilution. The value of E_a in the CH_2Br_2 systems at 60 mole percent amide was about 25 percent higher than the value of E_a in the CCl_4 systems at the same amide concentration.

Their interpretation of the results is the following:

1. The rather large energy barriers (9 kcal/mole for DMP and 7 kcal/mole for DMCC compared with 1.976 kcal/mole for methylamine) (4) can be attributed largely to the partial double-bond character of the C-N bond acquired through the following resonance structures:

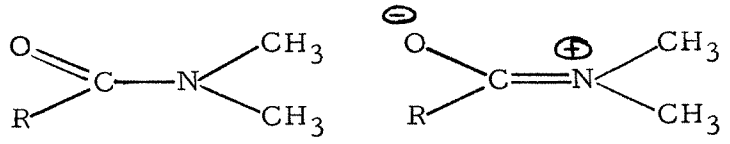

I II

The contribution of resonance structure II is favored by interactions of the type

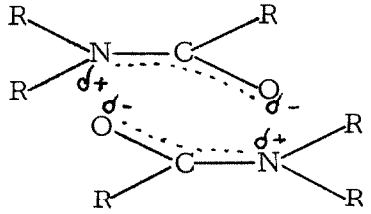

2. The dielectric constants of DMP, CCl_4, and CH_2Br_2 are approximately 28, 2.2, and 7 respectively at room temperature. In the case of the DMP-CCl_4 system dilution of DMP by CCl_4 will cause the above interaction to become increasingly less important. Thus resonance form II will become less favored, and the energy barrier will decrease, as was found to be the case.

3. For the DMP-CH_2Br_2 system hydrogen bonding of the type

$$HBr_2C-H \cdots O=CR'-NR_2$$

becomes important in favoring resonance structure II. As DMP is diluted the energy barrier is at first increased because of this hydrogen bonding. At further dilutions the decrease in the dielectric constant of the system becomes important and the energy barrier is decreased.

4. The lower rotational barrier for pure DMCC can be attributed to the resonance form

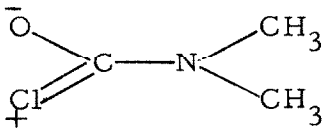

III

competing with resonance form II, thereby making form II less important. Dilution by a non-polar solvent would be expected to decrease the energy barrier less markedly than for DMP.

There are several objections to the above interpretations of the results. The authors have contributed the large increase in the energy barrier in the DMP- CH_2Br_2 system to an effect caused by hydrogen bonding. Yet by extrapolating their data to infinite dilution, there appears to be very little, if indeed any, difference in E_a. If the authors interpretation of the more or less constant energy barrier in the DMCC-CCl_4 system is correct, by the same argument one would expect the hydrogen bonding to have a lesser effect on E_a in the

DMCC–CH_2Br_2 system than in the DMP–CCl_4 system. However, the increase in the barrier was found to be about the same (possibly slightly more) in the DMCC–CH_2Br_2 system. These facts seem to indicate that the importance of hydrogen bonding was over estimated.

In explaining the reduced energy barrier in the case of DMCC, the authors ignore any possibility of a reduction in the internal rotational energy barrier by a reduction in steric hindrance in going from the ethyl group to the chlorine atom.

In order to help clarify some of the above problems the following two experiments are proposed. The system N, N–dimethylformamide–CCl_4 should be studied. In this way any effect from the steric hindrance of the ethyl group contributing to the internal rotational barrier about the C—N bond could be eliminated. Thus it could be determined whether or not resonance form III makes an important contribution to the energy barrier.

If a N, N–dimethylsubstituted amide–H_2O system were studied, the effects of hydrogen bonding could be better determined. Since H_2O has a fairly high dielectric constant (about 80), the dielectric constant of the solution would not decrease with increasing dilution of the amide. Also H_2O should be a better hydrogen bonder than CH_2Br_2, thus increasing any effect due to hydrogen bonding.

References

1. J. C. Woodbrey and M. T. Rogers, J. Am. Chem. Soc. 84, 13 (1962).

2. W. D. Phillips, J. Chem. Phys. 23, 1363 (1955).

3. H. S. Gutowsky and C. H. Holm, ibid. 25, 1228 (1956).

4. C. C. Lin and J. D. Swalen, Revs. Modern Phys. 31, 841 (1959).